Article

Nutrients activate distinct patterns of small-intestinal enteric neurons

https://doi.org/10.1038/s41586-025-09228-z

Received: 27 January 2023

Accepted: 3 June 2025

Published online: 09 July 2025

Open access

Check for updates

Candice Fung[1], Tom Venneman[1], Amy M. Holland[2,3], Tobie Martens[1], Milvia I. Alata[1], Marlene M. Hao[1,7], Ceyhun Alar[4,5], Yuuki Obata[6,8], Jan Tack[1], Alejandro Sifrim[4,5], Vassilis Pachnis[6], Werend Boesmans[2,3] & Pieter Vanden Berghe[1]✉

The ability to detect and respond appropriately to ingested nutrients is essential for an organism's survival and to ensure its metabolic demands are met. Nutrient signals from the gut lumen trigger local intestinal reflexes in the enteric nervous system (ENS) to facilitate digestion and absorption[1–4], but the precise cellular pathways that are involved in the initial neuronal sensory process remain unclear. The extent to which the ENS is capable of discerning different luminal chemicals is also unknown. Here we use calcium imaging to identify specific enteric pathways that are activated in response to luminal nutrients applied to mouse jejunum. Notably, we show that different nutrients activate neurochemically defined ensembles of myenteric and submucosal neurons. Furthermore, we find that enteric neurons are not directly sensitive to nutrients but detect different luminal chemicals through the epithelium, mainly via a serotonin signalling pathway. Finally, our data reveal a spatial distribution of luminal information along the radial axis of the intestine, whereby some signals that originate from the villus epithelium are transmitted first to the myenteric plexus, and then back to the submucosal plexus, which is closer to the lumen.

Monitoring of ingested nutrients by the gastrointestinal tract is crucial for energy homeostasis. Precise signalling of sensory cues from the intestinal lumen is key for guiding physiologically appropriate responses at not only at the organ but also the behavioural level. For instance, neuropod cells in the intestinal epithelium make specialized connections with the vagus nerve, which enables rapid gut–brain signalling and helps drive the preference for nutritive sugars over non-caloric sweeteners[5]. Sensory information from the gut also forms a key branch of visceral signals transmitted to the nodose ganglion to inform the brain of the body's overall internal state[6]. However, little is known about how sensory cues, even basic nutrients, are handled at the initial site of contact; namely, by the gut itself and its ENS. Different luminal compositions elicit distinct intestinal behaviours. A nutritious meal produces mixing motor patterns to facilitate digestion and absorption, whereas a non-caloric meal predominantly induces propulsive contractions[7]. When presented with cholera toxin[8] together with a nutritious fatty acid, the intestine apparently overrides signals to trigger mixing and rapidly evokes propulsive contractions, presumably prioritizing elimination of the diarrhoea-inducing agent[9]. Despite this, how luminal information is communicated to the ENS remains unclear, and the specific enteric pathways that allow the gut to distinguish between different luminal chemicals have yet to be identified.

The ENS comprises a repertoire of intrinsic primary afferent neurons (IPANs, or intrinsic sensory neurons), interneurons and motor neurons organized within two ganglionated plexuses: the submucosal plexus (SMP) and the myenteric plexus (MP)[3,4,10,11]. Because the epithelial barrier shields the luminal contents, how the ENS detects luminal cues is unclear. Although previous work has focused on various aspects of mechanosensation of the ingested bolus[12,13], and mucosal chemosensation[14–16], less is known about the communication and further processing of these epithelial signals in the ENS plexuses. Here we developed experimental strategies to record ENS activity in response to mucosal stimuli ex vivo and in vivo. We show that chemically distinct signals activate unique combinations of enteric neurons in register with the overlying villi. We uncover a stereotypic sequence of neuronal activation, in which some signals that originate from the villi are transmitted to neurons in the outer MP and then return to the inner SMP. The modular and hierarchical organization of signal-specific neuronal circuits activated by the exposure of villi to distinct chemicals provides a basis for understanding how the gut's luminal environment elicits meaningful physiological responses.

Villi receive local ENS innervation

To anatomically map the innervation of a villus, we injected a neuronal tracer, DiI, into the tip of a villus. Labelled myenteric and submucosal neurons were mostly in close vicinity to the labelled villus (71 ± 15% of labelled neurons situated within a 558-µm radius of the villus; Fig. 1a–d). This spatial arrangement of enteric neurons relative to the associated villus is in line with the developmental distribution of the related neuroglial progenitor cell lineage in radial columns along

[1]Laboratory for Enteric Neuroscience (LENS), Translational Research Center for Gastrointestinal Disorders (TARGID), KU Leuven, Leuven, Belgium. [2]Department of Pathology, GROW – Research Institute for Oncology and Reproduction, Maastricht, The Netherlands. [3]Biomedical Research Institute (BIOMED), Hasselt University, Diepenbeek, Belgium. [4]KU Leuven Institute for Single Cell Omics (LISCO), Leuven, Belgium. [5]Laboratory of Multi-omic Integrative Bioinformatics, Center for Human Genetics, KU Leuven, Leuven, Belgium. [6]Nervous System Development and Homeostasis Laboratory, Francis Crick Institute, London, UK. [7]Present address: Department of Anatomy and Physiology, University of Melbourne, Melbourne, Victoria, Australia. [8]Present address: University of Texas Southwestern Medical Center, Dallas, TX, USA. ✉e-mail: pieter.vandenberghe@kuleuven.be

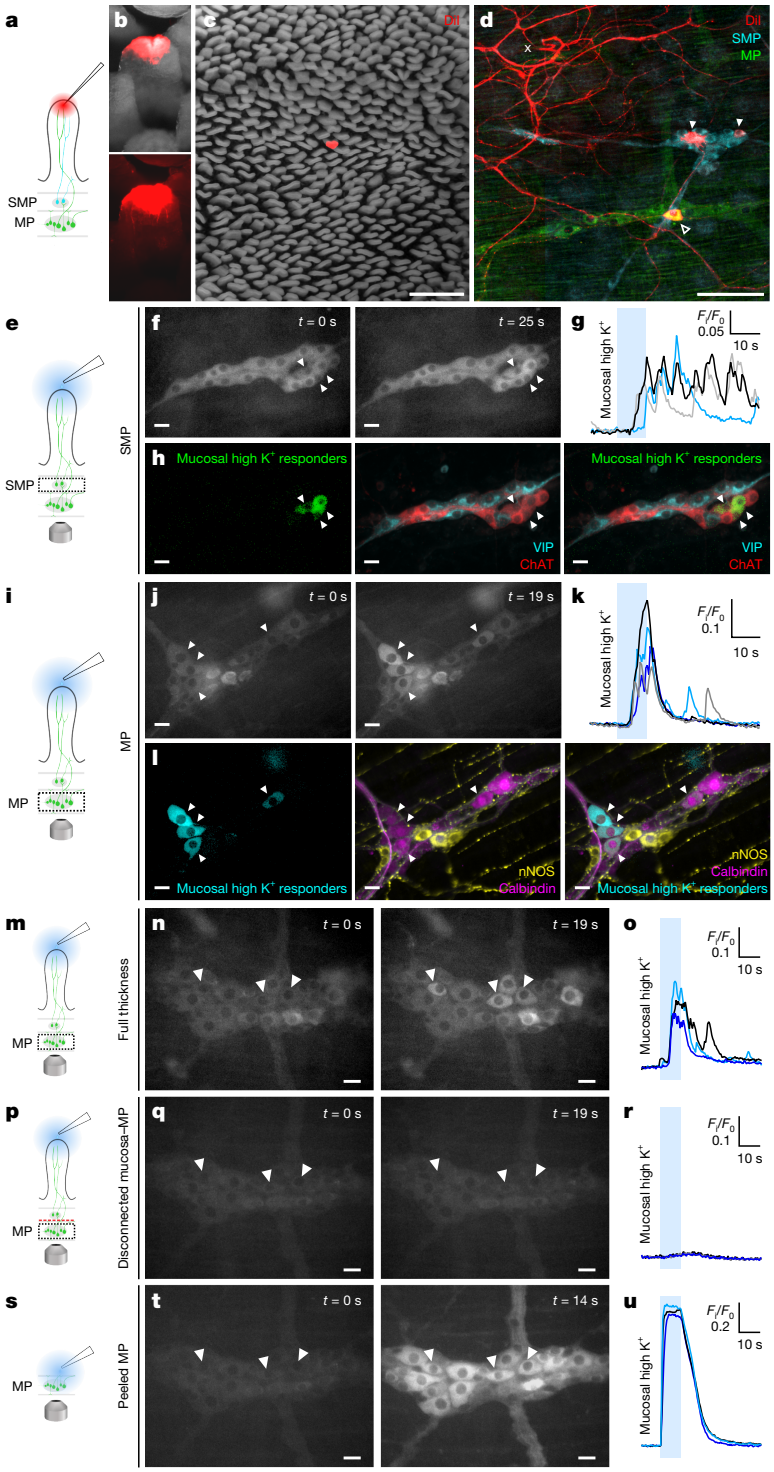

Fig. 1 | ENS responses to mucosal high K$^+$. **a**, DiI was injected into a single villus tip ($n = 3$ preparations). **b**, Representative DiI-labelled villus. **c**, Overview of the mucosa in a full-thickness preparation with a DiI-labelled villus. **d**, DiI-labelled nerve fibres and submucosal (cyan) and myenteric (green) (GCaMP-expressing) neurons (arrowheads). The point of DiI application is marked with an x. **e**,**i**, High-K$^+$ (75 mM) Krebs solution was perfused onto the mucosa at $t = 10$–20 s while imaging the underlying SMP (**e**) or MP (**i**). **f**,**j**, Submucosal (**f**) and myenteric (**j**) neurons responding (arrowheads) at $t = 0$ s (left panels), $t = 25$ s (**f**, right) and t = 19 s (**j**, right). **g**,**k**, Ca^{2+} transients in the indicated SMP (**g**) and MP (**k**) responders. **h**,**l**, Left, submucosal (**h**, green) and myenteric (**l**, cyan) responders. **h**, Middle, SMP immunolabelled for ChAT and VIP ($n = 4$ preparations). Right, responders included ChAT$^+$ submucosal neurons. **l**, Middle, MP immunolabelled for calbindin and neuronal nitric oxide synthase (nNOS) ($n = 4$ preparations). Right, responders included calbindin$^+$ myenteric neurons. **m**, Myenteric responses to mucosal high K$^+$ in the full-thickness preparation ($n = 3$ preparations). **n**, Selected responders (arrowheads) at $t = 0$ s (left) and $t = 19$ s (right). **o**, Ca^{2+} transients in the indicated responders. **p**–**r**, The same preparation was peeled apart between the circular muscle and the SMP, severing connections between the MP and the mucosa (**p**). The separated layers were replaced, and the mucosa was depolarized. Responses in the same ganglion were abolished after peeling. **q**, Responders at $t = 0$ s (left) and $t = 19$ s (right). **r**, Ca^{2+} transients. **s**–**u**, The mucosal layer was removed to expose the MP (**s**). The same neurons were directly exposed to high K$^+$ and depolarized. **t**, Responders at $t = 0$ s (left) and $t = 14$ s (right). **u**, Ca^{2+} transients. Scale bars, 1 mm (**c**), 100 µm (**d**) and 20 µm (**f**,**h**,**j**,**l**,**n**,**q**,**t**). Drawings in **a**,**e**,**i**,**m**,**p** and **s** are adapted from ref. 30 (Wiley).

the lumen–mucosa axis[17], and is consistent with findings in guinea pigs[18,19]. Having established the topographical organization of enteric neurons supplying a villus, we proceeded to examine the functionality of these neurons.

Mucosal high K^+ activates the ENS

Under physiological conditions, the gut epithelium is exposed to a plethora of chemical stimuli, which widely activate enteroendocrine cells (EECs), including serotonin (5-HT)-containing enterochromaffin (EC) cells[20–22]. A high K^+ (75 mM) Krebs solution was used to broadly stimulate these electrically excitable EECs[23,24], and the SMP and MP responses were examined in preparations of *Wnt1-Cre;R26R-LsL-GCaMP3* (Wnt1|GCaMP3) mouse jejunum (Fig. 1e–l). Mucosal high K^+ evoked Ca^{2+} transients in a subset of submucosal and myenteric neurons (24 ± 6% and 22 ± 3% of neurons examined, respectively). To further characterize these neurons, imaged preparations were labelled for choline acetyltransferase (ChAT) and vasoactive intestinal peptide (VIP) in the SMP, to distinguish between two major subtypes of submucosal secretomotor and vasodilator neurons[25]. Responders were mostly cholinergic ($ChAT^+$; Fig. 1f–h and Supplementary Table 1). In the MP, we labelled for calbindin, which is a commonly used marker for IPANs, and for nNOS, which is a marker for inhibitory interneurons and motor neurons[26]. Most myenteric responders were $calbindin^+$ and few were $nNOS^+$ (Fig. 1j–l and Supplementary Table 2), suggesting that IPANs and downstream nitrergic neurons were activated.

We then assessed whether MP–mucosa nerve connections are necessary for mucosal signal transmission. First, we verified that mucosal high K^+ could elicit responses in myenteric neurons in intact preparations (Fig. 1m–o). The gut layers were then peeled apart between the circular muscle and the SMP, severing MP–mucosa connections, and the separated layers were replaced. This abolished the responses to mucosal high K^+ in the ganglia that were imaged previously (Fig. 1p–r), indicating that the effect of high K^+ was not due to diffusion through the epithelium to the underlying MP. To confirm that the neurons were still viable after peeling, we showed that directly depolarizing the same ganglia evoked robust Ca^{2+} transients in nearly all neurons, including all initial responders (Fig. 1s–u). These data show that MP–mucosa and/or MP–SMP connections are essential for transmitting luminal signals.

Nutrients activate the ENS through the mucosa

To examine the effects of different luminal nutrients on ENS activity, nutrient solutions were applied to the mucosa while imaging the SMP or MP (Fig. 2). Glucose (300 mM; Supplementary Videos 1 and 2), acetate (100 mM; Supplementary Videos 3 and 4) and L-phenylalanine (L-Phe; 100 mM; Supplementary Videos 5 and 6) were selected as a model sugar, short-chain fatty acid and amino acid, respectively. Because glucose (11.5 mM) is present in the Krebs solution, glucose stimulation was considered as the increase from baseline to 300 mM. Krebs perfusion alone did not have any effects, demonstrating that the perfusion pressure applied was not a sufficient mechanical stimulus to evoke mechanosensory responses (Supplementary Tables 1 and 2).

In the SMP (Fig. 2a–l), glucose, acetate and L-Phe each activated a comparable percentage of mostly cholinergic ($ChAT^+$) neurons (21 ± 4%, 24 ± 7% and 23 ± 3%, respectively; Fig. 2j,k and Supplementary Table 1). Cell size was quantified as another means of classifying responders, because IPANs tend to have type II morphology with somas that are larger than those of other neurons[26]; this was also comparable between nutrients (Fig. 2l).

In the MP (Fig. 2m–x), glucose (300 mM) evoked responses in 17 ± 6% of neurons, which included $calbindin^+$, neuronal nitric oxide $synthase^+$ ($nNOS^+$) and $calbindin^-nNOS^-$ neurons, whereas acetate (100 mM) and L-Phe (100 mM) elicited responses in 10 ± 2% and 9 ± 2% of neurons, respectively, which included $calbindin^+$ and $calbindin^-nNOS^-$ neurons (Fig. 2v,w). The numbers of $calbindin^+$ and $nNOS^+$ neurons examined were comparable across preparations (Supplementary Table 2). However, the relative proportions of the neurochemical subtypes of responders ($P < 0.0001$; χ^2 test) and their cell diameters differed between stimuli (Fig. 2x), confirming that different nutrients activate unique ensembles of myenteric neurons.

To further characterize the molecular identity of nutrient-responsive myenteric neurons, RNAscope was performed, targeting specific populations informed by RNA sequencing (RNA-seq)-based classifications[27]. We labelled three putative myenteric IPAN populations (distinguished by *Nmu*, *Cck* or *Nxph2* expression). Nutrient-responsive neurons exhibited mainly *Nmu* (Extended Data Fig. 1), rarely *Cck* and never *Nxph2* expression (Supplementary Table 3).

To examine the differential response to nutrients, we applied each nutrient to the mucosa sequentially and imaged the same myenteric ganglion. Of the total responders, a small fraction were activated by all or various combinations of nutrients, and more than half responded uniquely to one nutrient (Extended Data Fig. 2); many were acetate-responsive. Because extracellular glucose concentration can influence myenteric neuronal excitability[28], glucose exposure might affect subsequent nutrient responses. The potential influence of one nutrient on responses to another should be taken into account when interpreting these data.

Considering nutrient transport or diffusion across the epithelium, we tested whether mucosal sensory nerves are directly nutrient sensitive. Glucose (300 mM), acetate (100 mM) or L-Phe (100 mM) were applied into a single villus, using a micropipette pushed through the epithelium, to target sensory nerve endings. Although 5-HT applied in this manner activates enteric neurons[29], this mode of nutrient application was not effective. Local nutrient application onto myenteric ganglia in peeled longitudinal muscle–myenteric plexus (LMMP) preparations also did not elicit neuronal responses (Supplementary Table 4). Thus, mucosal sensory nerves do not directly detect these nutrient solutions, indicating that the epithelium is necessary for initial sensory transduction of nutrient signals.

To verify that the epithelium senses these nutrients, we applied each nutrient solution onto the mucosal surface of jejunal preparations from *Villin-cre;R26R-LsL-GCaMP3* (Villin|GCaMP3) mice[30]. Nutrients and high K^+ elicited epithelial Ca^{2+} responses (Extended Data Fig. 3 and Supplementary Videos 7–9). Analysing published single-cell and single-nucleus RNA-seq datasets[27,31,32], we found clusters of small-intestinal epithelial cell types expressing genes that encode associated nutrient sensing receptors and transporters, putative neuroactive mediators and vesicular release proteins (Extended Data Fig. 4a).

Consistent with the glucose responses observed, where Ca^{2+} signals were widely distributed throughout the epithelial surface (Supplementary Video 7), *Slc5a1* (encoding the sodium–glucose co-transporter 1; SGLT1) and *Tas1r2* and *Tas1r3* (encoding components of the sweet taste receptor heterodimer T1R2–T1R3) were most highly expressed by enterocytes (the most abundant epithelial cell type). By contrast, acetate and L-Phe responses were confined mainly to distinct clusters of epithelial cells (Supplementary Videos 8 and 9). In accordance with this, expression of *Ffar2* (short-chain fatty acid receptor) was highest in EECs and goblet cells, which are constituents of a smaller population of secretory cells sparsely distributed throughout the epithelium. Similarly, expression of *Casr* (calcium-sensing receptor) and *Tas1r1* and *Tas1r3* (components of the taste receptor heterodimer T1R1–T1R3), each associated with sensing L-amino acids, was found predominantly in EECs and in goblet cells, respectively.

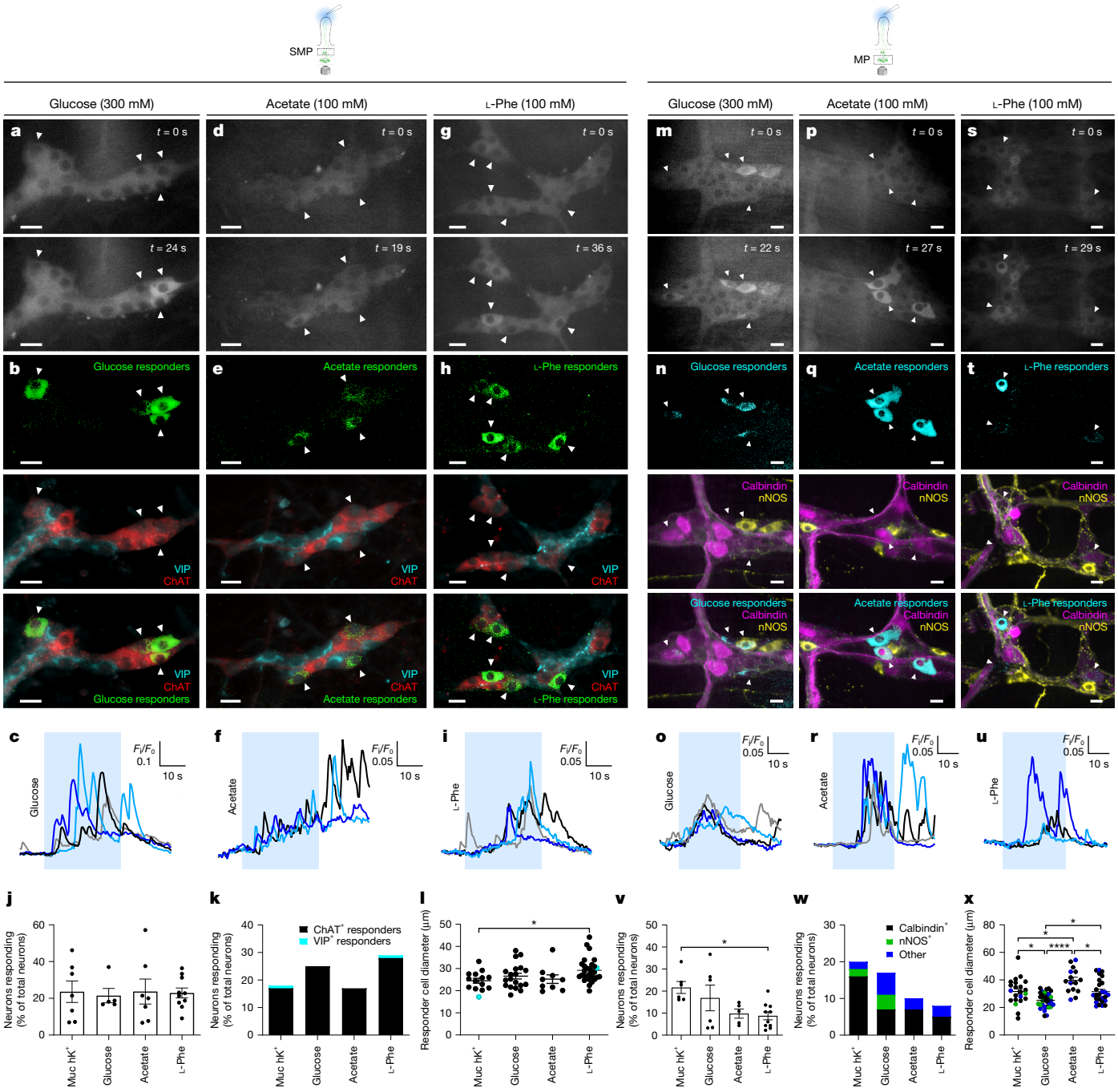

Fig. 2 | ENS responses to mucosal nutrient perfusion. a,**d**,**g**,**m**,**p**,**s**, Mucosal perfusion of glucose (**a**,**m**), acetate (**d**,**p**) or L-Phe (**g**,**s**) activates a subset of enteric neurons (arrowheads). Nutrients were applied at $t = 10–40$ s. **b**,**e**,**h**, Top, submucosal responders (green) to glucose (**b**), acetate (**e**) or L-Phe (**h**). Middle, submucosal ganglia were labelled for ChAT and VIP. Bottom, overlays demonstrate that submucosal responders were cholinergic. **n**,**q**,**t**, Top, myenteric responders (cyan) to glucose (**n**), acetate (**q**) or L-Phe (**t**). Middle, myenteric ganglia were labelled for calbindin and nNOS. Bottom, myenteric responders included calbindin$^+$ and nNOS$^+$ neurons. **c**,**f**,**i**, Ca^{2+} transients in submucosal responders to glucose (**c**), acetate (**f**) or L-Phe (**i**). **o**,**r**,**u**, Ca^{2+} transients in myenteric responders to glucose (**o**), acetate (**r**) or L-Phe (**u**). **j**, The percentage of submucosal neurons that responded to mucosal high K^+ (muc hK$^+$), glucose, acetate and L-Phe was comparable. $n = 5–10$ fields of view (FOVs) imaged. **k**, Submucosal responders were predominantly cholinergic. **l**, The cell diameter of responders was comparable between nutrients (ChAT$^+$, black; VIP$^+$, cyan). A difference was detected between muc hK$^+$ and L-Phe responders (*$P = 0.039$; one-way analysis of variance (ANOVA), Tukey's multiple comparisons test). $n = 4–6$ preparations. **v**, The percentage of myenteric responders to muc hK$^+$, glucose and acetate was comparable. L-Phe evoked a smaller response than muc hK$^+$ (*$P = 0.0334$; one-way ANOVA, Tukey's multiple comparisons test). $n = 5–10$ FOVs imaged. **w**, Many myenteric responders were calbindin$^+$. **x**, The cell diameter of myenteric responders differed between stimuli (*$P < 0.05$, **** $P < 0.0001$; one-way ANOVA, Tukey's multiple comparisons test; calbindin$^+$, black; nNOS$^+$, green; calbindin$^-$nNOS$^-$, blue). $n = 4–7$ preparations. Data are mean ± s.e.m. Scale bars, 20 µm. Drawings at the top are adapted from ref. 30 (Wiley).

Therefore, epithelial cells involved in nutrient signal transduction might not be limited to EECs, and could include other cell types.

To assess the importance of epithelium–ENS communication in transmitting nutrient information, we tested the effect of disrupting epithelial signalling on neuronal responses. Blocking SGLT1 with

mizagliflozin[33] (1 μM) attenuated glucose responses in the MP and SMP (Extended Data Fig. 5), suggesting that SGLT1 has a major role.

Mucosa–ENS signalling involves 5-HT

To identify mediators involved in transducing luminal signals to the ENS, we assessed the ability of molecules to activate enteric neurons through mucosal nerve endings. Putative mucosal mediators (5-HT, ATP, CCK8 and GLP-1; refs. 34,35) implicated in nutrient signalling were injected into villi (to mimic their basolateral release onto mucosal nerve endings) while imaging the MP (Fig. 3a and Supplementary Table 4).

5-HT–5-HT_3 signalling is considered to be a key mucosal sensory pathway involved in transducing chemical and mechanical stimuli in the gastrointestinal tract[1,13,24,36]. 5-HT puffed onto the mucosa stimulates myenteric neurons[37,38]. We found that intravillus injection of 5-HT (10 μM) evoked responses in 18 ± 10% myenteric neurons (Fig. 3a–e); many were calbindin$^+$ (Fig. 3d). In accordance with our previous findings[29], 5-HT acted through 5-HT_3 receptors, because its effect was abolished by ondansetron (10 μM) (Fig. 3e).

ATP is implicated as a mediator in mucosal mechanosensitivity[39]. Mucosal application of ATP activates myenteric afterhyperpolarization-type neurons in guinea-pig ileum through P2X receptors[40]. Here, intravillus injection of ATP (200 μM) activated 7 ± 2% of myenteric neurons, most of which were calbindin$^+$ (Fig. 3f–i). The P2X antagonist TNP-ATP (5 μM) inhibited the response (Fig. 3i).

In the jejunum, intravillus injection of CCK8 (100 nM) or GLP-1 (100 nM) had no effect, suggesting that the responses to intravillus injection of 5-HT or ATP were not due to mechanical stimulation. Considering the enrichment of CCK8-containing I cells in the duodenum and GLP-1-containing L cells in the terminal ileum, we also examined these regions. Unlike what was seen with 5-HT, no responses were observed when CCK8 was injected into duodenal villi or when GLP-1 was injected into terminal ileum villi (Extended Data Fig. 6a–f). GLP-1 might stimulate intestinofugal neurons in the ileum that have mucosal projections[35]. We could have missed these neurons, because they form only a small proportion of myenteric neurons and tend to be situated along the mesenteric border. We also cannot rule out the possibilities that these mediators target extrinsic mucosal nerve endings or that they modulate activity within the plexus. Indeed, CCK8 or GLP-1 applied onto jejunal LMMP activated some myenteric neurons (Extended Data Fig. 6g–j).

On the basis of an analysis of single-cell and single-nucleus RNA-seq datasets of small-intestinal enteric neurons[27,32], *Htr3a* and *P2rx2* are highly expressed in IPANs, as defined by *Calcb*, *Calb2* and *Nmu* expression (Extended Data Fig. 4b). This is compatible with our RNAscope data, in which many nutrient responders expressed *Nmu* (Extended Data Fig. 1). These neurons showed low levels of *Glp1r*, *Cckar*, *Cckbr* and *Calb1* expression, despite the fact that calbindin is a commonly used marker for IPANs[26]. Because the calbindin antibody used might cross-react with calretinin[27], calcitonin gene-related peptide (CGRP) was used as an additional IPAN marker. CGRP immunoreactivity is normally observed only in varicosities, so tissues were cultured in colchicine to disrupt axonal transport and concentrate the peptide in the soma before immunostaining[41]. In colchicine-treated tissues, 85 ± 11% of CGRP-immunoreactive myenteric neurons were labelled with the calbindin antibody (Extended Data Fig. 7).

Having found that mucosal nerve endings were responsive to 5-HT and ATP, we tested for endogenous 5-HT and ATP release after the application of mucosal high K$^+$, using ondansetron (10 μM) and TNP-ATP (5 μM) (Fig. 3j–k). Ondansetron inhibited but did not abolish the response, indicating the activation of a 5-HT–5-HT_3 receptor-independent pathway. On the other hand, TNP-ATP had no effect, demonstrating that ATP acting through P2 receptors is not involved.

Chemosensitive myenteric IPANs

Although mucosal high K$^+$ activates calbindin$^+$ myenteric neurons, suggesting that these are IPANs, it is unclear whether they respond directly or synaptically. This was addressed using the nicotinic antagonist hexamethonium (Hex, 200 μM) to block the major form of excitatory neurotransmission in the ENS (Fig. 4a,b). The percentage of myenteric neurons activated before and after Hex exposure was comparable, which indicates that responders (observed locally within the field of view, FOV) were activated directly.

With repeated mucosal high K$^+$ application, the second stimulation activated significantly more myenteric neurons (Fig. 4a, left). These additional responders were mainly calbindin$^+$, nNOS$^+$, or calbindin$^-$nNOS$^-$ neurons with smaller cell bodies than those of the initial responders (Fig. 4a, right), and were probably excitatory and inhibitory motor neurons and/or interneurons. The amplified response with the second mucosal high K$^+$ application was inhibited by Hex (Fig. 4b), demonstrating that the additional neurons were recruited through nicotinic neurotransmission.

Because direct and synaptic responses to mucosal high K$^+$ were observed, we set out to characterize the myenteric neurons functionally connected to an individual villus with a more localized stimulus using a focal electrode (Fig. 4c–g). Train stimulation (20 Hz, 1 s) in control and Hex conditions elicited reproducible responses in 14 ± 5% of myenteric neurons (Supplementary Table 4). Like the initial mucosal high K$^+$ responders, electrical stimulation responders were predominantly calbindin$^+$ (Fig. 4d–f). In the Hex condition, a total of 89 ± 7% of initial responders were activated by the second electrical stimulation, whereas the same numbers responded to both stimulations in control conditions (Fig. 4g). The effect of electrical stimulation was therefore mainly direct, with a minor component being synaptic, and 14 ± 5% of myenteric neurons within the FOV functionally innervate a single villus. This is comparable to the numbers of myenteric responders to intravillus 5-HT injection (16 ± 4%), suggesting that most (if not all) mucosal nerve endings are sensitive to 5-HT.

Responses to mucosal high K$^+$ in both plexuses were examined simultaneously using spinning disk confocal microscopy (Extended Data Fig. 8). The Ca^{2+} transient peak in the initial myenteric responder typically preceded that of the initial submucosal responder (Extended Data Fig. 8a–c).

Chemosensitive submucosal IPANs

To examine whether submucosal responses to mucosal high K$^+$ occur directly or synaptically, we applied Hex (Fig. 4h,i). Repeated mucosal high K$^+$ evoked consistent responses in control conditions (Fig. 4h), and these were partly reduced but not abolished by Hex (Fig. 4i), suggesting that non-nicotinic synaptic signalling or direct activation are also involved[42].

Because submucosal but not myenteric responders to mucosal high K$^+$ were Hex sensitive, we assessed the extent to which the SMP receives myenteric inputs. We compared the submucosal responses to electrical stimulation of a single villus with and without the MP. First, a train stimulus (20 Hz, 1 s) was applied to the villus with a focal electrode in an intact preparation, which activated a subset of submucosal neurons (Fig. 4j–l). The same villus (marked by DiI) was then stimulated after removing the MP (Fig. 4m–q), and the response was significantly reduced (Fig. 4o–r). Thus, some submucosal neurons were activated secondarily through the MP. Because responses were still observed after removing the MP, these neurons might be activated directly (IPANs) and/or by antidromic transmission (secretomotor neurons). Repeated electrical stimulation in intact preparations elicited reproducible responses (Fig. 4r).

To determine whether the SMP contains IPANs, we applied nutrients onto mucosa–SMP preparations (Extended Data Fig. 9). Glucose, acetate and L-Phe activated 22 ± 4%, 6 ± 2% and 7 ± 3% of submucosal

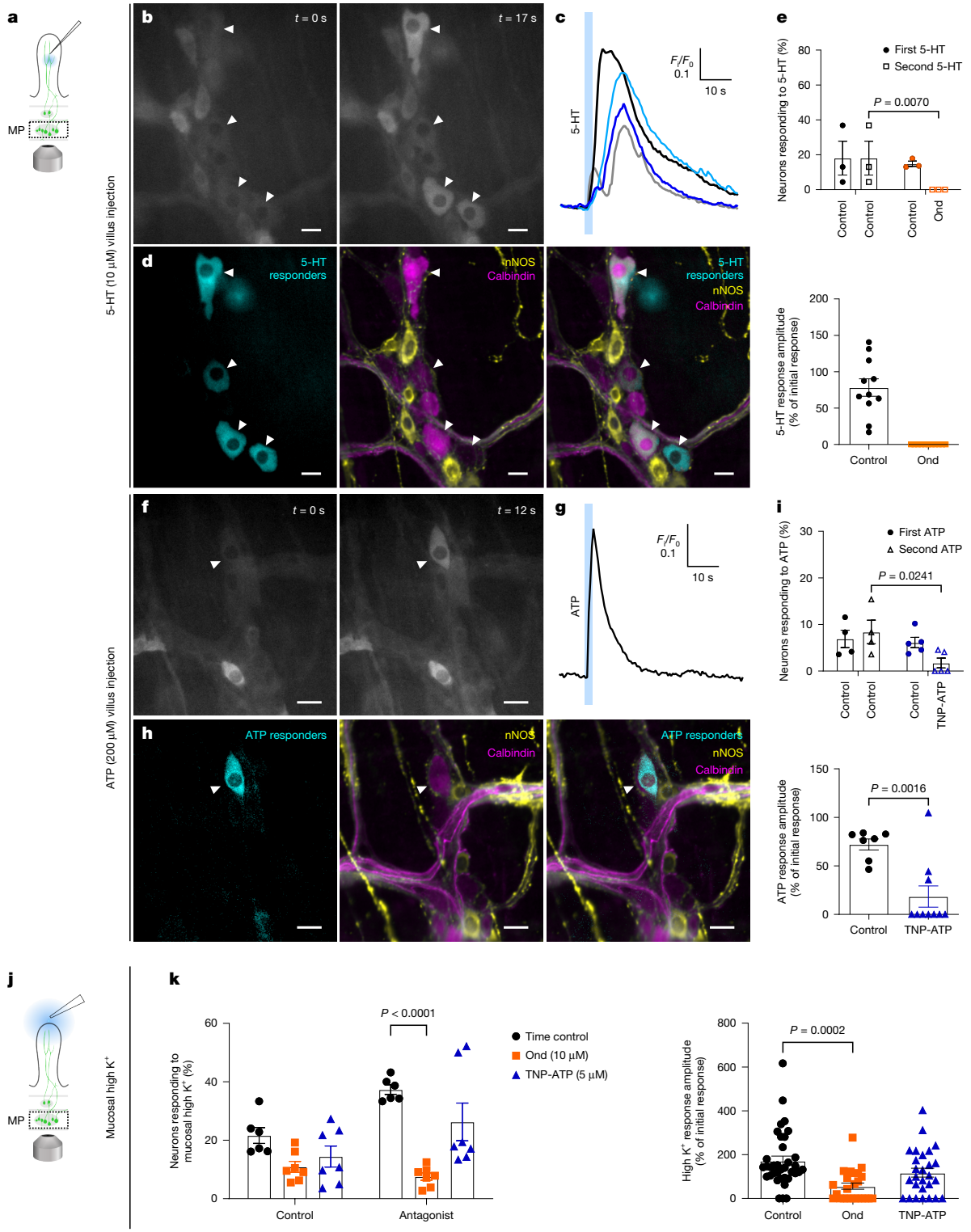

Fig. 3 | Mucosal nerve endings are sensitive to 5-HT and ATP. a, The MP was imaged while 5-HT or ATP was injected into a single villus. **b**,**f**, 5-HT (**b**) and ATP (**f**) activated a subset of neurons (arrowheads). **c**,**g**, Ca^{2+} transients in 5-HT (**c**) and ATP (**g**) responders. Agonists were applied at $t = 10$ s. **d**,**h**, Left, responders (cyan) to 5-HT (**d**) and ATP (**h**). Middle, immunolabelling for calbindin and nNOS. Right, overlays show that many 5-HT and ATP responders were calbindin$^+$. **e**,**i**, Repeated 5-HT (**e**) or ATP (**i**) injections evoked reproducible responses under control conditions. **e**, The 5-HT response was abolished by ondansetron (Ond, 10 µM) in terms of the percentage of responders (top, two-way ANOVA, Šídák's multiple comparisons test, $n = 3$ preparations examined) and the response amplitude (bottom, two-sided unpaired t-test). **i**, The ATP response was significantly reduced by TNP-ATP (5 µM) in terms of the percentage of responders (top, two-way ANOVA, Šídák's multiple comparisons test, $n = 4$–5) and the response amplitude (bottom, two-sided unpaired t-test). **j**, Stimulating or antagonist solutions were perfused onto the mucosal surface. **k**, Left, the percentage of myenteric responders to mucosal high K^+ was significantly reduced by ondansetron (10 µM), but not by TNP-ATP (5 µM), when compared with the corresponding control time point (two-way ANOVA, Sidak's multiple comparisons test, $n = 5$–7). Right, response amplitudes were reduced by ondansetron (10 µM), but not by TNP-ATP (5 µM) (one-way ANOVA, Sidak's multiple comparisons test). Data are mean ± s.e.m. Scale bars, 20 µm. Drawings in **a** and **j** are adapted from ref. 30 (Wiley).

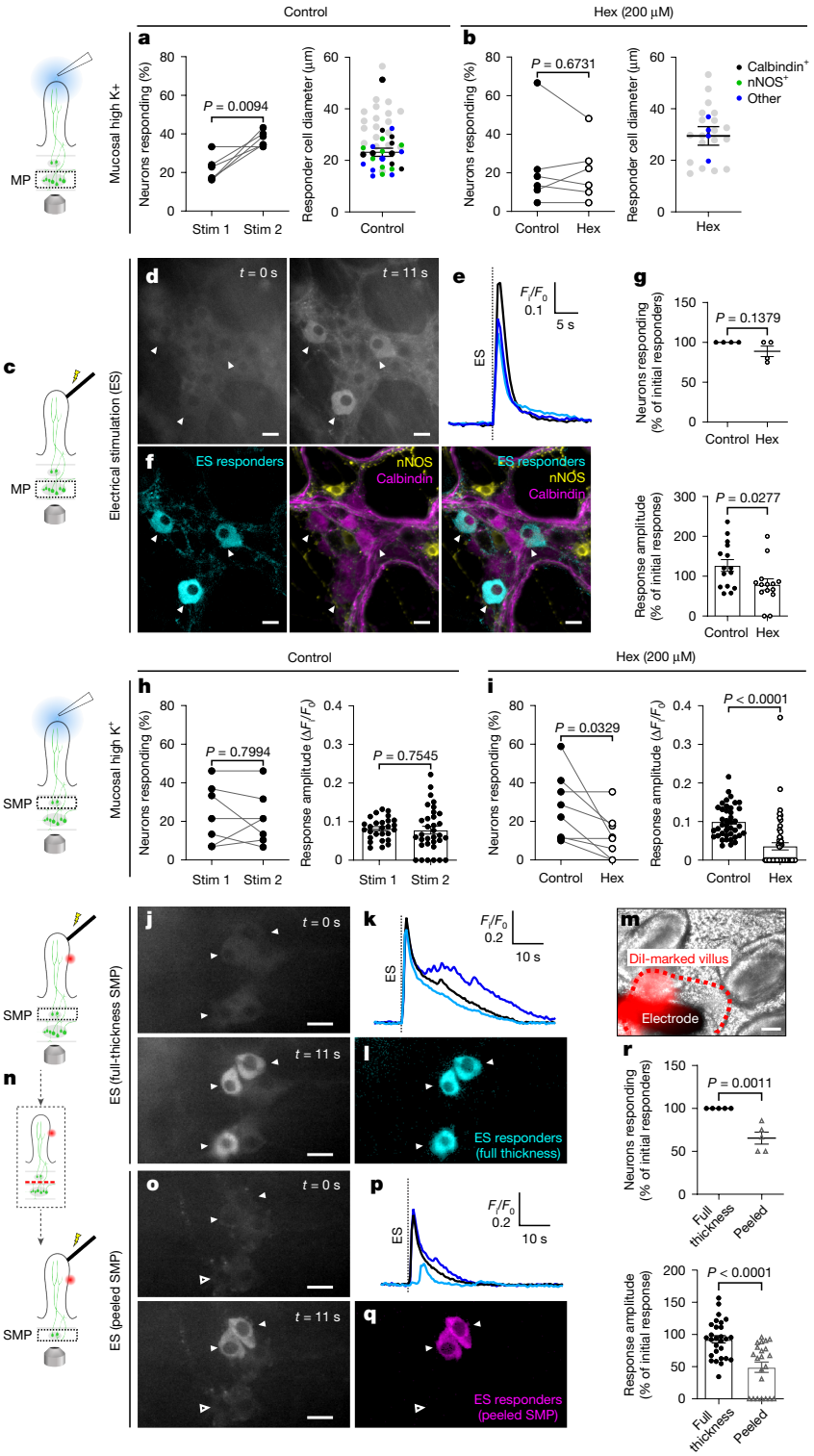

Fig. 4 | Mucosal stimulation activates IPANs and synaptic responses. a, Left, repeated mucosal high K^+ application evoked reproducible responses in the MP, with an increase in the number of responders with the second stimulation (Stim) (two-sided paired *t*-test, $n = 6$ FOVs). Right, cell diameter of new responders (blue, green and black) and initial responders (grey). **b**, Left, the percentage of responders to the second stimulus was unaffected by Hex (two-sided paired *t*-test, $n = 6$ FOVs). Right, few new responders (blue, $nNOS^-calbindin^-$) were observed with Hex. **c**, Train stimulation (20 Hz, 1 s) of a villus using a focal electrode. **d**, MP responders (arrowheads). **e**, Ca^{2+} transients in responders. The stimulus was applied at $t = 10$ s. **f**, Left, electrical stimulation (ES) responders (cyan). Middle, immunolabelling for calbindin and nNOS. Right, some responders were $calbindin^+$. **g**, The percentage of responders was comparable between control and Hex conditions (top), but response amplitudes were reduced by Hex (bottom) (two-sided unpaired t-test, $n = 4$ FOVs). **h**,**i**, Mucosal high K^+ evoked reproducible responses in the SMP (**h**, $n = 7$ FOVs); responses were inhibited by Hex (**i**, $n = 8$ FOVs) (two-sided paired *t*-test). **j**, Submucosal responses to electrical stimulation of a villus (20 Hz, 1 s) in a full-thickness preparation (arrowheads). **k**, Ca^{2+} transients in responders. The stimulus was applied at $t = 10$ s. **l**, ES responders (cyan). **m**,**n**, The stimulated villus was marked with DiI (red) (image (**m**) and schematic (**n**)). **o**, DiI-marked villus was stimulated after removing the MP. A subset of initial responders were activated. **p**, Ca^{2+} transients in the indicated neurons. **q**, Responders (magenta). **r**, Responses were reduced after removing the MP (two-sided unpaired *t*-test, $n = 5$ preparations per condition). Data are mean ± s.e.m. Scale bars, 20 µm. Drawings in **a**,**c**,**h**,**j** and **n** are adapted from ref. 30 (Wiley).

neurons, respectively, providing evidence for submucosal IPANs. However, fewer neurons were stimulated by acetate and L-Phe in peeled than in full-thickness preparations, indicating that myenteric inputs contribute to submucosal responses to acetate and L-Phe, but not glucose.

Nutrient-induced ENS responses in vivo

Several factors can influence local nutrient responses, including long-range nerve projections within the ENS, extrinsic innervation, blood flow, the presence of mucus, the gut microbiota, and pancreatic and hepatic signals. We examined the integrated system by imaging the ENS in vivo (Fig. 5). As a proof of concept, we luminally applied nutrient solution into an externalized jejunal loop of an anaesthetized mouse and imaged the MP. Consistent with our ex vivo data, acetate (100 mM) acutely activated a subset of myenteric neurons in the jejunal loop in vivo (15 ± 2% of neurons) (Supplementary Video 10); these included calbindin$^+$ and nNOS$^+$ neurons (6/30 and 13/30 responders, respectively). Because the imaging site is around 5 mm distal of the nutrient perfusion site, downstream motor neurons and interneurons are likely to have been visualized as well as IPANs. Some neurons might be sensitive to distension from perfusion, because luminal Krebs also evoked Ca^{2+} responses[43] (in 7 ± 2% of neurons); many were nNOS$^+$ (6/9 responders).

Discussion

Here, using Ca^{2+} imaging, we have shown that specific enteric pathways are activated by luminal chemicals, and that the ENS can decipher intraluminal contents, with distinct ensembles of neurons responding to different nutrients ex vivo. Similar results were observed when nutrients were applied into an externalized jejunal loop in live mice. Our findings pave the way to a better understanding of how the intestine monitors the luminal chemical environment and how luminal cues shape its functional output. Although further work will be necessary to fully characterize how luminal information is coded and communicated to the ENS, our findings corroborate previous studies that have identified 5-HT as a key molecule mediating signalling between the epithelium and myenteric IPANs through 5-HT_3 receptors[38,44]. Because enterocytes and EC cells in the mouse small intestine lack neuropods[45], their communication with nerve endings must involve another mechanism. Previous work indicates that mucosal 5-HT is likely to act through paracrine signalling[46]. In olfactory sensation, most odours are encoded not by one receptor, but by a pattern of receptors and olfactory receptor neurons[47]. It is likely that different luminal stimuli are similarly encoded by patterns of mediators in addition to 5-HT and depend on combinations of epithelial mediators and corresponding neuronal receptors.

Across all modes of mucosal stimulation, calbindin$^+$CGRP$^+$ *Nmu*-expressing myenteric neurons were prominent responders, in line with the initial responders to luminal signals being myenteric IPANs[26,27,48]. Downstream of myenteric IPANs are myenteric interneurons, motor neurons and submucosal neurons activated through nicotinic transmission (Extended Data Fig. 10). Studies suggest that IPANs are also present in the mouse SMP, on the basis of neuronal morphology, projection patterns, advillin expression[49] and RNA-seq data[32]. Indeed, we observed submucosal responses to nutrients even without the MP, adding functional evidence for submucosal IPANs. Antidromic activation was unlikely, because cholinergic and VIPergic submucosal neurons supplying the mucosa are abundant[25], but responders were almost exclusively cholinergic. Mucosal stimulation also activates some submucosal neurons through the MP, in agreement with previous work that showed that submucosal neurons receive nicotinic inputs from myenteric neurons[50]. Myenteric neurons might, in turn, receive inputs from submucosal neurons[51]. This bidirectional signalling is likely to be important in coordinating intestinal motility, secretion and blood flow for optimizing digestion and absorption[52]. Collectively, nutrient signals locally activate submucosal and myenteric sensory circuits, as well as motor circuits, and some myenteric neurons converge onto submucosal pathways.

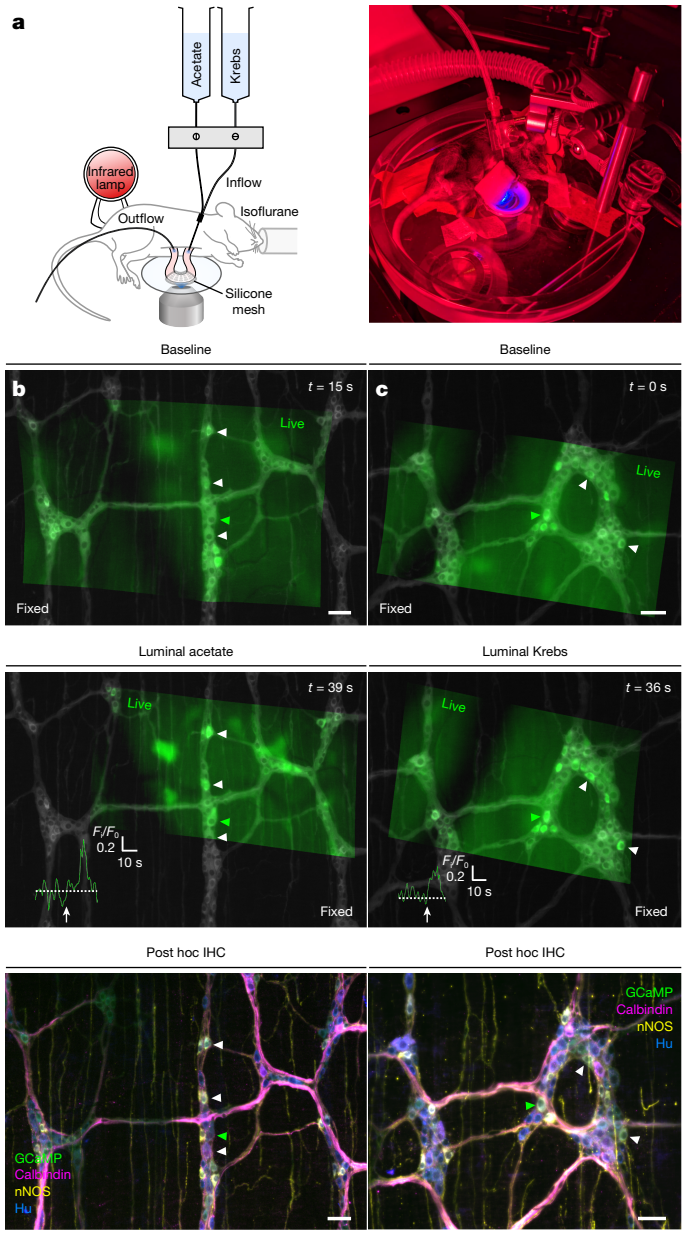

Fig. 5 | Myenteric neuronal responses to luminal acetate in the jejunum of a live mouse. a, Schematic (left; adapted from ref. 30 (Wiley)) and imaging set-up (right) for Ca^{2+} imaging of enteric neuronal activity in response to luminal infusion of nutrient solution in a loop of mouse jejunum in vivo. The mouse was anaesthetized using isoflurane and its body temperature was maintained using an infrared lamp. Flexible tubing was inserted into a loop of jejunum proximal to the imaging site to infuse nutrient (acetate, 100 mM; $n = 3$ mice) or Krebs solution (control; $n = 2$ mice), and distal to the imaging site for the outflow of solution. The jejunal loop was stabilized using a custom-designed silicone mesh. **b**,**c**, Top, acetate (**b**) or Krebs solution (**c**) was applied, and examples of responding neurons are indicated (arrowheads). Frames from the live recording (green overlay, live) are mapped onto an image of the fixed MP (greyscale, fixed) using a semi-automated registration strategy. Middle, traces depict Ca^{2+} transients in the responding neurons (green arrowheads). The start of acetate or Krebs application is marked with white arrows. Bottom, with post hoc immunolabelling (immunohistochemistry; IHC) of imaged myenteric neurons (Hu$^+$), acetate responders included calbindin$^+$ and nNOS$^+$ neurons (**b**), whereas Krebs infusion activated nNOS$^+$ neurons (**c**). Scale bars, 50 µm.

Our study shows that the MP is a key site of initial luminal signal processing and integration, despite the fact that it is physically further away from the lumen than is the SMP. Additional processing occurs in the SMP, in which neurons receive luminal information directly, and via the MP. This spatial organization of sensory circuits might reflect a functional advantage, in which priority is assigned to initiating motility programs and the initial responders are those that are close to the target smooth muscle. The ENS of lower vertebrates, such as zebrafish, comprises a MP layer but lacks a SMP[53], suggesting that fine-tuned secretomotor and vasomotor control evolved later. We speculate that myenteric neurons are evolutionarily wired to rapidly process luminal signals, and that this is conserved across species. Further studies will be necessary to determine the full extent of neuronal activation beyond the stimulation site—with regard to not only downstream enteric interneurons and motor neurons, but also extrinsic nerves—and establish how the net activity ultimately translates into complex intestinal behaviours.

Online content

Any methods, additional references, Nature Portfolio reporting summaries, source data, extended data, supplementary information, acknowledgements, peer review information; details of author contributions and competing interests; and statements of data and code availability are available at https://doi.org/10.1038/s41586-025-09228-z.

1. Bertrand, P. P. The cornucopia of intestinal chemosensory transduction. *Front. Neurosci.* **3**, 48 (2009).
2. Neunlist, M. & Schemann, M. Nutrient-induced changes in the phenotype and function of the enteric nervous system. *J. Physiol.* **592**, 2959–2965 (2014).
3. Fung, C. & Vanden Berghe, P. Functional circuits and signal processing in the enteric nervous system. *Cell. Mol. Life Sci.* **77**, 4505–4522 (2020).
4. Furness, J. B. The enteric nervous system and neurogastroenterology. *Nat. Rev. Gastroenterol. Hepatol.* **9**, 286–294 (2012).
5. Buchanan, K. L. et al. The preference for sugar over sweetener depends on a gut sensor cell. *Nat. Neurosci.* **25**, 191–200 (2022).
6. Zhao, Q. et al. A multidimensional coding architecture of the vagal interoceptive system. *Nature* **603**, 878–884 (2022).
7. Schemann, M. & Ehrlein, H. J. Postprandial patterns of canine jejunal motility and transit of luminal content. *Gastroenterology* **90**, 991–1000 (1986).
8. Nocerino, A., Iafusco, M. & Guandalini, S. Cholera toxin-induced small intestinal secretion has a secretory effect on the colon of the rat. *Gastroenterology* **108**, 34–39 (1995).
9. Fung, C., Ellis, M. & Bornstein, J. C. Luminal cholera toxin alters motility in isolated guinea-pig jejunum via a pathway independent of 5-HT_3 receptors. *Front. Neurosci.* **4**, 162 (2010).
10. Schneider, S., Wright, C. M. & Heuckeroth, R. O. Unexpected roles for the second brain: enteric nervous system as master regulator of bowel function. *Annu. Rev. Physiol.* **81**, 235–259 (2019).
11. Spencer, N. J. & Hu, H. Enteric nervous system: sensory transduction, neural circuits and gastrointestinal motility. *Nat. Rev. Gastroenterol. Hepatol.* **17**, 338–351 (2020).
12. Mercado-Perez, A. & Beyder, A. Gut feelings: mechanosensing in the gastrointestinal tract. *Nat. Rev. Gastroenterol. Hepatol.* **19**, 283–296 (2022).
13. Alcaino, C. et al. A population of gut epithelial enterochromaffin cells is mechanosensitive and requires Piezo2 to convert force into serotonin release. *Proc. Natl Acad. Sci. USA* **115**, E7632–E7641 (2018).
14. Furness, J. B., Rivera, L. R., Cho, H.-J., Bravo, D. M. & Callaghan, B. The gut as a sensory organ. *Nat. Rev. Gastroenterol. Hepatol.* **10**, 729 (2013).
15. Husted, A. S., Trauelsen, M., Rudenko, O., Hjorth, S. A. & Schwartz, T. W. GPCR-mediated signaling of metabolites. *Cell Metab.* **25**, 777–796 (2017).
16. Worthington, J. J., Reimann, F. & Gribble, F. M. Enteroendocrine cells-sensory sentinels of the intestinal environment and orchestrators of mucosal immunity. *Mucosal Immunol.* **11**, 3–20 (2018).
17. Lasrado, R. et al. Lineage-dependent spatial and functional organization of the mammalian enteric nervous system. *Science* **356**, 722–726 (2017).
18. Song, Z. M., Brookes, S. J. & Costa, M. Identification of myenteric neurons which project to the mucosa of the guinea-pig small intestine. *Neurosci. Lett.* **129**, 294–298 (1991).
19. Song, Z. M., Brookes, S. J., Steele, P. A. & Costa, M. Projections and pathways of submucous neurons to the mucosa of the guinea-pig small intestine. *Cell Tissue Res.* **269**, 87–98 (1992).
20. Martin, A. M. et al. The nutrient-sensing repertoires of mouse enterochromaffin cells differ between duodenum and colon. *Neurogastroenterol. Motil.* **29**, e13046 (2017).
21. Martin, A. M. et al. Regional differences in nutrient-induced secretion of gut serotonin. *Physiol. Rep.* **5**, e13199 (2017).
22. Gribble, F. M. & Reimann, F. Function and mechanisms of enteroendocrine cells and gut hormones in metabolism. *Nat. Rev. Endocrinol.* **15**, 226–237 (2019).
23. Rogers, G. J. et al. Electrical activity-triggered glucagon-like peptide-1 secretion from primary murine L-cells. *J. Physiol.* **589**, 1081–1093 (2011).
24. Bellono, N. W. et al. Enterochromaffin cells are gut chemosensors that couple to sensory neural pathways. *Cell* **170**, 185–198 (2017).
25. Mongardi Fantaguzzi, C., Thacker, M., Chiocchetti, R. & Furness, J. B. Identification of neuron types in the submucosal ganglia of the mouse ileum. *Cell Tissue Res.* **336**, 179–189 (2009).
26. Qu, Z. D. et al. Immunohistochemical analysis of neuron types in the mouse small intestine. *Cell Tissue Res.* **334**, 147–161 (2008).
27. Morarach, K. et al. Diversification of molecularly defined myenteric neuron classes revealed by single-cell RNA sequencing. *Nat. Neurosci.* **24**, 34–46 (2021).
28. Liu, M., Seino, S. & Kirchgessner, A. L. Identification and characterization of glucoresponsive neurons in the enteric nervous system. *J. Neurosci.* **19**, 10305 (1999).
29. Hao, M. M. et al. Development of the intrinsic innervation of the small bowel mucosa and villi. *Am. J. Physiol. Gastrointest. Liver Physiol.* **318**, G53–G65 (2020).
30. Fung, C. et al. Luminal short chain fatty acids and 5-HT acutely activate myenteric neurons in the mouse proximal colon. *Neurogastroenterol. Motil.* **33**, e14186 (2021).
31. Haber, A. L. et al. A single-cell survey of the small intestinal epithelium. *Nature* **551**, 333–339 (2017).
32. Drokhlyansky, E. et al. The human and mouse enteric nervous system at single-cell resolution. *Cell* **182**, 1606–1622 (2020).
33. Inoue, T. et al. Mizagliflozin, a novel selective SGLT1 inhibitor, exhibits potential in the amelioration of chronic constipation. *Eur. J. Pharmacol.* **806**, 25–31 (2017).
34. Akalestou, E. et al. Intravital imaging of islet Ca^{2+} dynamics reveals enhanced β cell connectivity after bariatric surgery in mice. *Nat. Commun.* **12**, 5165 (2021).
35. Zhang, T., Perkins, M. H., Chang, H., Han, W. & de Araujo, I. E. An inter-organ neural circuit for appetite suppression. *Cell* **185**, 2478–2494 (2022).
36. Gershon, M. D. & Tack, J. The serotonin signaling system: from basic understanding to drug development for functional gi disorders. *Gastroenterology* **132**, 397–414 (2007).
37. Bertrand, P. P., Kunze, W. A., Bornstein, J. C., Furness, J. B. & Smith, M. L. Analysis of the responses of myenteric neurons in the small intestine to chemical stimulation of the mucosa. *Am. J. Physiol.* **273**, G422–G435 (1997).
38. Bertrand, P. P., Kunze, W. A., Furness, J. B. & Bornstein, J. C. The terminals of myenteric intrinsic primary afferent neurons of the guinea-pig ileum are excited by 5-hydroxytryptamine acting at 5-hydroxytryptamine-3 receptors. *Neuroscience* **101**, 459–469 (2000).
39. Cooke, H. J., Wunderlich, J. & Christofi, F. L. 'The force be with you': ATP in gut mechanosensory transduction. *News Physiol. Sci.* **18**, 43–49 (2003).
40. Bertrand, P. P. & Bornstein, J. C. ATP as a putative sensory mediator: activation of intrinsic sensory neurons of the myenteric plexus via P2X receptors. *Neuroscience* **22**, 4767–4775 (2002).
41. Vanden Berghe, P. et al. Neurochemical coding of myenteric neurons in the guinea-pig antrum. *Cell Tissue Res.* **297**, 81–90 (1999).
42. Pan, H. & Gershon, M. D. Activation of intrinsic afferent pathways in submucosal ganglia of the guinea pig small intestine. *J. Neurosci.* **20**, 3295–3309 (2000).
43. Mazzuoli-Weber, G. & Schemann, M. Mechanosensitivity in the enteric nervous system. *Front. Cell. Neurosci.* **9**, 408 (2015).
44. Gershon, M. D. in *The Enteric Nervous System II* (eds Spencer, N. J. et al.) 307–318 (Springer, 2022).
45. Koo, A., Fothergill, L. J., Kuramoto, H. & Furness, J. B. 5-HT containing enteroendocrine cells characterised by morphologies, patterns of hormone co-expression, and relationships with nerve fibres in the mouse gastrointestinal tract. *Histochem. Cell Biol.* **155**, 623–636 (2021).
46. Touhara, K. K. et al. Topological segregation of stress sensors along the gut crypt–villus axis. *Nature* **640**, 732–742 (2025).
47. Su, C. Y., Menuz, K. & Carlson, J. R. Olfactory perception: receptors, cells, and circuits. *Cell* **139**, 45–59 (2009).
48. Furness, J. B., Jones, C., Nurgali, K. & Clerc, N. Intrinsic primary afferent neurons and nerve circuits within the intestine. *Prog. Neurobiol.* **72**, 143–164 (2004).
49. de Souza Melo, C. G. et al. Identification of intrinsic primary afferent neurons in mouse jejunum. *Neurogastroenterol. Motil.* **32**, e13989 (2020).
50. Moore, B. A. & Vanner, S. Properties of synaptic inputs from myenteric neurons innervating submucosal S neurons in guinea pig ileum. *Am. J. Physiol. Gastrointest. Liver Physiol.* **278**, G273–G280 (2000).
51. Monro, R. L., Bornstein, J. C. & Bertrand, P. P. Synaptic transmission from the submucosal plexus to the myenteric plexus in guinea-pig ileum. *Neurogastroenterol. Motil.* **20**, 1165–1173 (2008).
52. Vanden Berghe, P. & Fung, C. in *The Enteric Nervous System II* (eds Spencer, N. J. et al) 71–79 (Springer, 2022).
53. Heanue, T. A., Shepherd, I. T. & Burns, A. J. Enteric nervous system development in avian and zebrafish models. *Dev. Biol.* **417**, 129–138 (2016).

Methods

Mice and tissue preparation

Adult C57BL/6, *Wnt1-Cre;R26R-LsL-GCaMP3* (Wnt1|GCaMP3) and *Villin-cre;R26R-LsL-GCaMP3* (Villin|GCaMP3) mice aged at least six weeks old and of either sex were euthanized by cervical dislocation. The mice used in this study were maintained on a normal diet (Sniff; Soest) and water was provided ad libitum. All procedures were approved by the Animal Ethics Committee of the University of Leuven (Belgium). Wnt1|GCaMP3 mice express the fluorescent Ca^{2+} indicator GCaMP3 in all enteric neurons and glia, whereas GCaMP3 is expressed in the gut epithelium in Villin|GCaMP3 mice[54–56].

Five-centimetre pieces of duodenum, jejunum and/or ileum were collected and immersed in Krebs solution (120.9 mM NaCl, 5.9 mM KCl, 1.2 mM $MgCl_2$, 1.2 mM NaH_2PO_4, 14.4 mM $NaHCO_3$, 11.5 mM glucose and 2.5 mM $CaCl_2$) bubbled with 95% oxygen and 5% carbon dioxide. Each intestinal segment was opened by cutting along the mesenteric border and pinned flat with the mucosal side up in a silicone-elastomer-coated dish. The intestinal contents were removed with Krebs washes and any remnants were carefully removed using forceps. Experiments were limited to a maximum of three hours after tissue collection to minimize potential effects of compromised mucosal integrity.

For Ca^{2+} imaging of neuronal activity, either full-thickness preparations of Wnt1|GCaMP3 tissues with all the layers of the intestinal wall intact or microdissected submucosal preparations with the mucosa intact were stretched across an inox ring with the plexus facing up and stabilized with an outer rubber O-ring[57]. By mechanically restricting gut movement in this manner, chemical blockade of smooth-muscle activity (that is, with nifedipine or nicardipine) was not necessary. Up to four ring preparations were obtained from each jejunal segment. Because we cut open the gut tube along the mesenteric border and positioned the anti-mesenteric side within the ring preparation for imaging, intestinofugal neurons, which typically have their cell bodies situated along the mesenteric border and form only a small proportion of total myenteric neurons[58–61], were probably under-sampled.

In some experiments, the connections between the MP and the submucosa were severed by peeling apart the gut layers between the SMP and the circular muscle. The two separate layers were then positioned back in place and mounted between the rings. For peeled LMMP preparations, the mucosa, SMP and circular muscle were removed by microdissection and the remaining layers were mounted between rings.

For labelling of CGRP, segments of jejunum from C57BL/6 mice were collected and dissected in sterile Krebs. Peeled MP preparations with the mucosa and submucosa removed were cultured overnight at 37 °C (5 % CO_2) in DMEM/F-12 (Thermo Fisher Scientific) containing penicillin (250 U ml^{-1}; Thermo Fisher Scientific), streptomycin (250 µg ml^{-1}; Thermo Fisher Scientific), glutamine, nifedipine (1 µM; Sigma), 2% fetal bovine serum (FBS; Sigma) and colchicine (to concentrate proteins in the neuronal cell soma; 100 µM; Sigma).

DiI labelling to trace enteric neurons innervating a single villus

Ring preparations were placed in a glass-coverslip-bottomed dish and constantly perfused with Krebs solution bubbled with 95% oxygen and 5% carbon dioxide. Preparations were viewed using a 20× objective on a Zeiss Axiovert 200M microscope. DiI (in 100% ethanol) was applied by pressure ejection (Picospritzer II; 10 psi, 2 s; General Valve Corporation) using a micropipette (tip diameter of 10–20 µm) pushed through the epithelial layer and into a single villus. Tissues were then removed from the rings, stretched and pinned flat and fixed in 4% paraformaldehyde in phosphate-buffered saline (PBS) for two hours at room temperature. This was followed by three 10-min washes in PBS, and tissues were then incubated in PBS at 37 °C for up to three weeks after DiI application.

Live Ca^{2+} imaging of epithelial activity

Villin|GCaMP3 tissues that were stretched and pinned flat with the mucosal side up in a silicone-elastomer-coated dish were continuously superfused with Krebs solution bubbled with 95% oxygen and 5% carbon dioxide throughout the experiment and imaged at room temperature. Imaging was performed using a Leica M165 FC fluorescent stereomicroscope (Leica) fitted with an X-Cite 200DC stabilized fluorescence light source (Lumen Dynamics) and an ORCA-Flash4.0 V3 digital CMOS camera (Hamamatsu). The mucosa was perfused with stimulating solutions using a micropipette tip positioned at the edge of the imaged FOV. Perfusion was achieved through a gravity-assisted tubing system. Recordings were acquired at 2 Hz for a duration of 2 min, and there was at least 5 min between each stimulus application.

Live Ca^{2+} imaging of neuronal activity

Ring preparations were kept at room temperature in a glass-coverslip-bottomed dish and constantly perfused with Krebs solution bubbled with 95% oxygen and 5% carbon dioxide throughout the experiment. Live Ca^{2+} imaging of Wnt1|GCaMP3 ring preparations was performed using either a wide-field or a spinning disk confocal microscopy set-up. Some preparations were imaged using a 20× objective on a Zeiss Axiovert 200M microscope, equipped with a monochromator (Poly V) and a cooled CCD camera (Imago QE) (TILL Photonics). Images were acquired using TILLVISION software (TILL Photonics). A separate set of experiments was performed using an Andor Revolution spinning disk confocal microscope (Andor) equipped with a Nikon 20× lens (NA 0.8). GCaMP3 was excited at 488 nm and 3-dimensional (3D) stacks (21–29 µm) were acquired using a Piezo Z Stage controller.

Mucosal application of nutrient stimuli. Glucose (300 mM), acetate (100 mM) or L-Phe (100 mM) were locally applied for 30 s onto the mucosal surface with a perfusion pipette positioned above the imaged myenteric or SMP, exposing entire villi within the local FOV (445 × 337 μm^2) to the nutrient solution. High-K^+ (75 mM) Krebs solution was applied onto the mucosa for 10 s to broadly depolarize EECs and EC cells, which are electrically excitable. For some experiments, tissues were perfused with various antagonists for 10 min before the second mucosal stimulus. For experiments involving the sequential application of different nutrient solutions to the same ganglia, each nutrient application was separated by 10 min Krebs perfusion and the order of nutrient application was alternated between experiments.

Spritz application of agonist into a single villus. To mimic the basolateral release of mucosal mediators, 5-HT, ATP, CCK8 or GLP-1 were applied by pressure ejection (Picospritzer II; 10 psi, 2 s; General Valve Corporation) using a micropipette (tip diameter of 10–20 µm) pushed through the epithelial layer and into a single villus as previously described[29].

Electrical stimulation. To stimulate the nerve endings in a single villus, a train of 300-µs pulses (20 Hz, 1 s, 30 V) was applied using a focal electrode (50-µm-diameter tungsten wire) gently lowered onto the villus tip, coupled to a Grass stimulation unit. The lipophilic tracer DiI (dissolved in ethanol) was applied onto the epithelium of villi by pressure ejection (Picospritzer II; 10 psi, 1 s) as a means of marking and relocating a single villus.

In vivo ENS Ca^{2+} imaging

Adult male Wnt1|GCaMP3 mice aged at least 12 weeks were used for in vivo imaging of the ENS. Mice were fasted for four hours before the surgical procedure. Mice were anaesthetized using isoflurane (2–3%) by inhalation until loss of the pedal withdrawal reflex. Anaesthesia was maintained (around 1.5% isoflurane) throughout the surgical and imaging procedure. Bupivacaine hydrochloride (0.05%) was

locally administered to the site of abdominal incision. A laparotomy was then performed and a 3–4-cm jejunal loop with as little gut contents as possible was exposed. The intestinal loop was positioned in a coverslip-bottomed imaging dish filled with Krebs solution containing nifedipine (1 μM) to reduce smooth-muscle contractions. The intestinal segment was further stabilized using a custom-designed 3D-printed biocompatible silicone mesh, which was attached to the coverslip. For the infusion of stimulating solutions into the lumen, a small incision was made along the anti-mesenteric border, avoiding major blood vessels. The tip of a flexible feeding tube (22 ga; Instech) was then inserted through the incision and into the lumen, before sealing off the opening using surgical glue (Vetbond). The feeding tube was then connected to perfusion lines containing Krebs or acetate (100 mM). A second incision was made distal to the intestinal loop positioned in the imaging dish to insert tubing allowing for the outflow of perfused solutions. Wet gauze was placed over the segment of exposed intestine not submerged in the solution of the imaging dish to avoid the tissue drying out. Enteric neuronal activity was imaged using a 20× objective on a Zeiss Axiovert 200M microscope as described above. The mice were euthanized by cervical dislocation after imaging and the imaged jejunal loop was dissected out and fixed for post hoc immunohistochemistry.

Recordings were stabilized in Fiji using the Descriptor-based series registration plug-in[62] and/or the Landmark Correspondences plug-in (transformation method, moving least squares; transformation class, affine) to overlay the recording onto a template image of the fixed and peeled MP.

Nutrients and drugs

Glucose (300 mM; Millipore) was prepared in distilled water. Acetate (100 mM) was prepared with acetic acid (100 mM; EMSURE) in a modified Krebs solution (in which the concentration of NaCl was reduced to 20 mM) and neutralized using NaOH (1 M). L-Phe (100 mM; Sigma) was also prepared in a modified Krebs solution with the concentration of NaCl adjusted to maintain the osmolarity. The pH of the nutrient solutions was adjusted to 7.4. The concentrations of nutrient solutions were selected to be within the range that is typically ingested. For instance, popular sweetened beverages contain around 300 mM glucose[63], vinegar can contain up to 1.17 M acetic acid[64] and the concentration of L-Phe in beef is around 70 mmol per kg (ref. 65).

5-HT (Sigma), ATP (Tocris), GLP-1 (7-36)-amide (Phoenix Pharmaceuticals), CCK8 (PolyPeptide Laboratories), hexamethonium bromide (Sigma), ondansetron (Sigma), TNP-ATP (Tocris) and mizagliflozin (MedChemExpress) were prepared as stock solutions and diluted to the final concentration using standard Krebs solution.

Analysis

Ca^{2+} imaging analyses were performed with custom-written routines in Igor Pro (WaveMetrics)[66]. Regions of interest were drawn over each cell to calculate the average $[Ca^{2+}]_i$ signal intensity. Values were then normalized to the baseline fluorescence intensity (F_i/F_0). Responses were considered when the $[Ca^{2+}]_i$ signal increased above baseline by at least five times the intrinsic noise. $[Ca^{2+}]_i$ peaks were calculated for each response, with the peak amplitude taken as the maximum increase in $[Ca^{2+}]_i$ from baseline ($\Delta F_i/F_0$). Image overlays highlighting responding neurons (activity-over-time images) were generated in Igor Pro. Image overlays highlighting active regions of Ca^{2+} activity in *Villin-cre;R26R-LsL-GCaMP3* tissues were created in Fiji using the AQuA plug-in[67]. The images presented were adjusted for brightness and contrast. Quantification of the cell diameters of neuronal responders was performed in Fiji.

Immunohistochemistry

After Ca^{2+} imaging experiments, some full-thickness ring preparations were fixed in 4% formaldehyde in PBS for 90 min at room temperature, followed by three 10-min washes in PBS. Fixed tissues were first separated into SMP and MP preparations by microdissection. The SMP was isolated by dissecting the submucosa and mucosa from the underlying muscle and myenteric layers, and the mucosa was then gently scraped off. MP preparations were obtained by removing the circular muscle from the remaining preparation.

Cultured colchicine-treated MP tissues were fixed in 4% formaldehyde in PBS for 60 min at room temperature, followed by three 10-min washes in PBS. The circular muscle was then removed by microdissection before immunostaining.

SMP and MP preparations were then processed for immunohistochemistry. Tissues were incubated first in a blocking solution for two hours at room temperature (4% donkey serum and 0.5% Triton X-100) and then in primary antisera (Supplementary Table 5) for 48–72 h at 4 °C. Tissues were washed in PBS (three 10-min washes) before incubating in secondary antisera (Supplementary Table 5) for two hours at room temperature, and then washed again (three 10-min washes in PBS) before mounting onto slides using Citifluor.

RNAscope

After Ca^{2+} imaging experiments, some full-thickness ring preparations were dissected to isolate the MP layer and then fixed in 4% paraformaldehyde in PBS for 24 h at 4 °C, followed by three 10-min washes in PBS. Fixed myenteric preparations were further dissected to remove the circular muscle by microdissection before further processing for fluorescence in situ hybridization using the RNAscope Multiplex Fluorescent Reagent Kit v2 assay according to the manufacturer's instructions. Protease III was used to digest the whole-mount preparations. The RNAscope probes (Advanced Cell Diagnostics) used were Nmu-C1 (446831), Cck-C2 (402271) and Nxph2-C3 (870131). After hybridization, tissues were counterstained for DAPI (Invitrogen; 62248) and/or GFP and mounted using VECTASHIELD Antifade Mounting Medium with DAPI (VectorLabs; H-1200-10) or with Citifluor.

Imaging immunolabelled, DiI-labelled or RNAscope-labelled tissues

Labelled preparations were viewed under either an epifluorescence microscope (Olympus BX41) with an Olympus XM10 camera, or a Zeiss Axio Imager M2 with an Axiocam 705 (Zeiss). Images were acquired using Photoshop software or ZEN Blue, and were adjusted for contrast and brightness before overlay and quantification. The Landmark Correspondences plug-in in Fiji (transformation method, moving least squares; transformation class, affine) was used to transform the image of immunolabelled preparations for overlay with the activity-over-time image highlighting responding neurons from Ca^{2+}-imaging recordings. Colchicine-treated tissues, DiI-labelled tissues and RNAscope-labelled tissues were also imaged on an LSM 780 confocal microscope (Zeiss) using a water-immersion 25x objective (NA 0.8, Zeiss). Some RNAscope-labelled tissues were imaged on an LSM 880 confocal microscope (Zeiss) using an oil-immersion 40× objective (Zeiss). Confocal micrographs display maximum projections of confocal *z*-stacks. Images were adjusted for brightness and contrast. Neuronal cell counts and analysis of DiI-labelled preparations were performed in ImageJ–Fiji.

Data and statistics

Data are presented as mean ± s.e.m. At least three mice were used for each set of experiments, unless stated otherwise. Two-sided *t*-tests were performed. One-way ANOVA or two-way ANOVA followed by a multiple comparisons test was used to determine statistical significance. Where appropriate, the *P* values presented were adjusted to account for multiple comparisons. $P < 0.05$ was considered significant. Analyses were performed using GraphPad Prism.

Analysis of RNA-seq data

Single-cell and single-nucleus RNA-seq datasets were downloaded from the Single Cell Portal (SCP44 (ref. 31) and SCP1038 (ref. 32)) and

the Sequence Read Archive (SRP135960). The data were analysed in R (v.4.1.2) using the Seurat (v.4.1.0) package. All data were normalized using standard Seurat normalization: for each cell the gene counts were divided by total counts and multiplied by a scaling factor of 10^4, followed by log transformation. The data were subsequently scaled gene-wise using Seurat's ScaleData function. The metadata from the original publications were used as cluster and cell-type annotations. Genes relating to nutrient sensing and transport, synaptic release, and neurotransmitters, neuropeptides and hormones, as well as their corresponding receptors, were selected for further downstream analysis. Violin plots for these genes were generated using Seurat's VlnPlot function with basic parameters.

Reporting summary

Further information on research design is available in the Nature Portfolio Reporting Summary linked to this article.

Data availability

All datasets analysed in this study are available in the main text and supplementary information. For Ca^{2+} imaging analysis, the source code and installation instructions can be found at ref. 66 'Source code 1' (https://doi.org/10.7554/eLife.42914.039; Ca^{2+} imaging analysis source code) and 'Source code 2' (https://doi.org/10.7554/eLife.42914.040; installation instructions and user guide). None of the materials mentioned in this study have use restrictions for which material transfer agreements (MTAs) are required. Source data are provided with this paper.

54. Zariwala, H. A. et al. A Cre-dependent GCaMP3 reporter mouse for neuronal imaging in vivo. *J. Neurosci.* **32**, 3131–3141 (2012).
55. Danielian, P. S., Muccino, D., Rowitch, D. H., Michael, S. K. & McMahon, A. P. Modification of gene activity in mouse embryos in utero by a tamoxifen-inducible form of Cre recombinase. *Curr. Biol.* **8**, 1323–1326 (1998).
56. el Marjou, F. et al. Tissue-specific and inducible Cre-mediated recombination in the gut epithelium. *Genesis* **39**, 186–193 (2004).
57. Vanden Berghe, P., Kenyon, J. L. & Smith, T. K. Mitochondrial Ca^{2+} uptake regulates the excitability of myenteric neurons. *J. Neurosci.* **22**, 6962–6971 (2002).
58. Furness, J. B., Koopmans, H. S., Robbins, H. L. & Lin, H. C. Identification of intestinofugal neurons projecting to the coeliac and superior mesenteric ganglia in the rat. *Auton. Neurosci.* **83**, 81–85 (2000).
59. Tan, L. L., Bornstein, J. C. & Anderson, C. R. The neurochemistry and innervation patterns of extrinsic sensory and sympathetic nerves in the myenteric plexus of the C57Bl6 mouse jejunum. *Neuroscience* **166**, 564–579 (2010).
60. Timmermans, J.-P. et al. Occurrence, distribution and neurochemical features of small intestinal neurons projecting to the cranial mesenteric ganglion in the pig. *Cell Tissue Res.* **272**, 49–58 (1993).
61. Tassicker, B. C., Hennig, G. W., Costa, M. & Brookes, S. J. H. Rapid anterograde and retrograde tracing from mesenteric nerve trunks to the guinea-pig small intestine in vitro. *Cell Tissue Res.* **295**, 437–452 (1999).
62. Preibisch, S., Saalfeld, S., Schindelin, J. & Tomancak, P. Software for bead-based registration of selective plane illumination microscopy data. *Nat. Methods* **7**, 418–419 (2010).
63. Ventura, E. E., Davis, J. N. & Goran, M. I. Sugar content of popular sweetened beverages based on objective laboratory analysis: focus on fructose content. *Obesity* **19**, 868–874 (2011).
64. Akiba, Y. et al. Short-chain fatty acid sensing in rat duodenum. *J. Physiol.* **593**, 585–599 (2015).
65. Reitelseder, S. et al. Phenylalanine stable isotope tracer labeling of cow milk and meat and human experimental applications to study dietary protein-derived amino acid availability. *Clin. Nutr.* **39**, 3652–3662 (2020).
66. Li, Z. et al. Regional complexity in enteric neuron wiring reflects diversity of motility patterns in the mouse large intestine. *eLife* **8**, e42914 (2019).
67. Wang, Y. et al. Accurate quantification of astrocyte and neurotransmitter fluorescence dynamics for single-cell and population-level physiology. *Nat. Neurosci.* **22**, 1936–1944 (2019).

Acknowledgements We thank M. Moons and L. Grammet for technical assistance; P. Van Veldhoven for the Villin-Cre mice; and members of the Laboratory for Enteric Neuroscience (LENS) for advice. This work was supported by grants from KU Leuven (METH/014/05; C.F., P.V.B. and J.T.); the Research Foundation Flanders (FWO) (G012223N (P.V.B.) and W001620N (W.B.)); the Dutch Research Council (NOW) (VIDI 016.196.367; W.B.); the European Union's Horizon 2020 research and innovation programme H2020-FETPROACT-2018-01, CONNECT (grant agreement 824070; C.F. and P.V.B.) and FAIR CHARM H2020, industrial leadership (ICT) project (grant agreement 101016457; C.F., M.I.A. and P.V.B.). Images were recorded on microscopy equipment in LENS and the Cell and Tissue Imaging Cluster (CIC) supported by the Hercules Foundation (AKUL/11/37, AKUL/09/50 and G093818N; P.V.B. and W.B.).

Author contributions C.F., P.V.B., W.B. and V.P. contributed to the conception or design of the work. C.F., A.M.H., T.M., T.V., M.I.A., M.M.H., C.A., A.S. and P.V.B. contributed to the acquisition, analysis and/or interpretation of data. C.F. performed the DiI tracing, ex vivo and in vivo imaging and immunolabelling experiments. T.V. assisted with the image registration of in vivo recordings. A.M.H., C.F. and T.M. performed the RNAscope labelling experiments and imaging. C.A. performed the analysis of published RNA-seq datasets. C.F., C.A., V.P., W.B. and P.V.B. contributed to the original draft. C.F., M.M.H., Y.O., J.T., A.S., V.P., W.B. and P.VB. contributed to the revision and editing of the final manuscript.

Competing interests The authors declare no competing interests.

Additional information

Supplementary information The online version contains supplementary material available at https://doi.org/10.1038/s41586-025-09228-z.

Correspondence and requests for materials should be addressed to P. Vanden Berghe.

Peer review information *Nature* thanks Ivan de Araujo, Michael Gershon and the other, anonymous, reviewer(s) for their contribution to the peer review of this work. Peer reviewer reports are available.

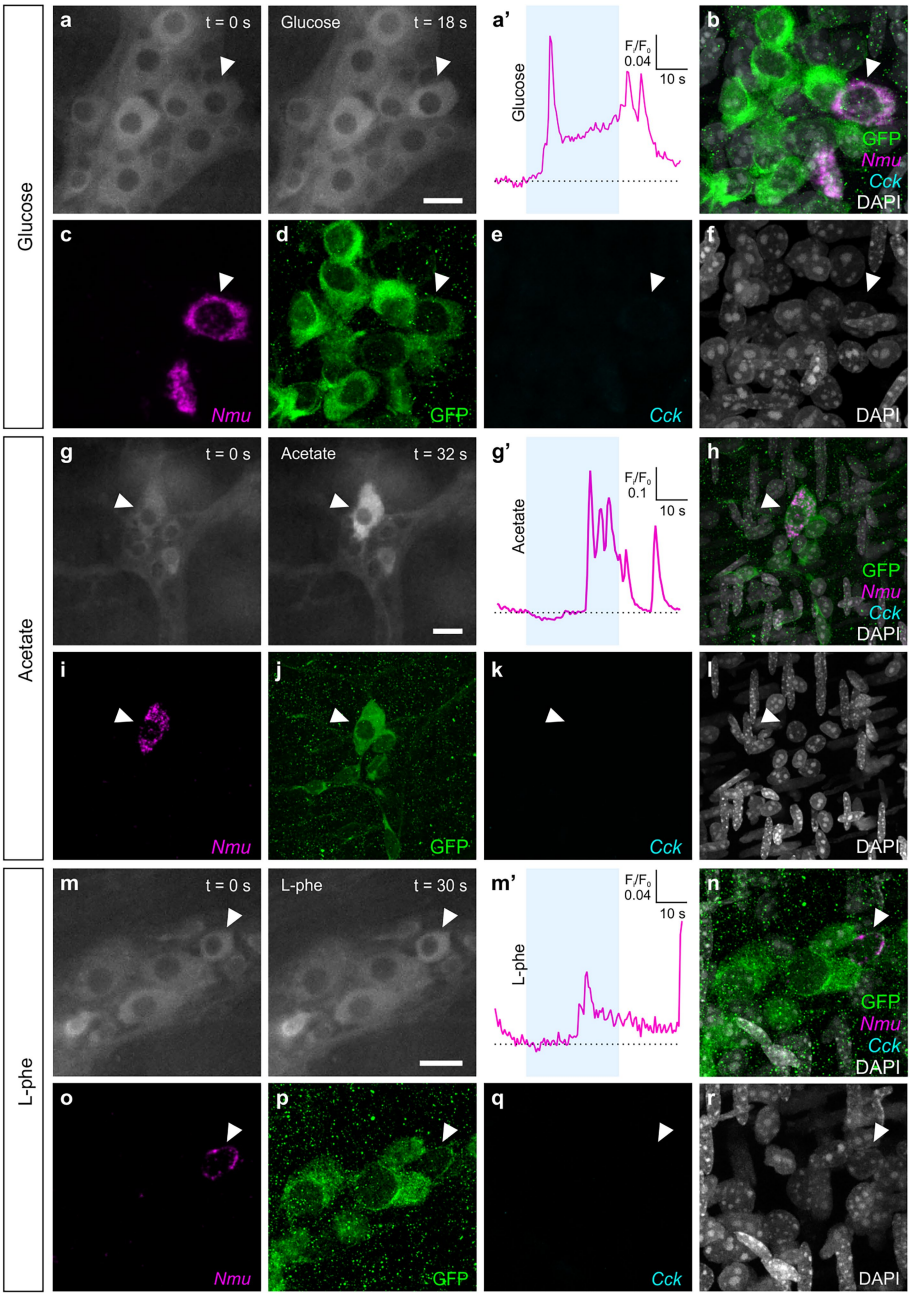

Extended Data Fig. 1 | Many nutrient-responsive myenteric neurons express *Nmu*. **a**–**r**, Myenteric (GCaMP$^+$GFP$^+$) neurons which responded to the mucosal application of glucose (300 mM) ($n = 2$ ganglia, $N = 2$ mice) (**a**–**f**), acetate (100 mM) ($n = 4$ ganglia; $N = 3$ mice) (**g**–**l**) and L-Phe (100 mM) ($n = 6$ ganglia; $N = 4$ mice) (**m**–**r**) together with the corresponding RNAscope labelling for *Nmu* and *Cck*. Tissues were immunostained with anti-GFP to enhance the GCaMP signal after RNAscope and nuclei were counterstained with DAPI. Scale bars, 20 µm. Ca^{2+} transients in the nutrient-responsive neurons (arrowheads) are also shown (**a'**,**g'**,**m'**). Nutrient solutions were applied from $t = 10$ s to $t = 40$ s.

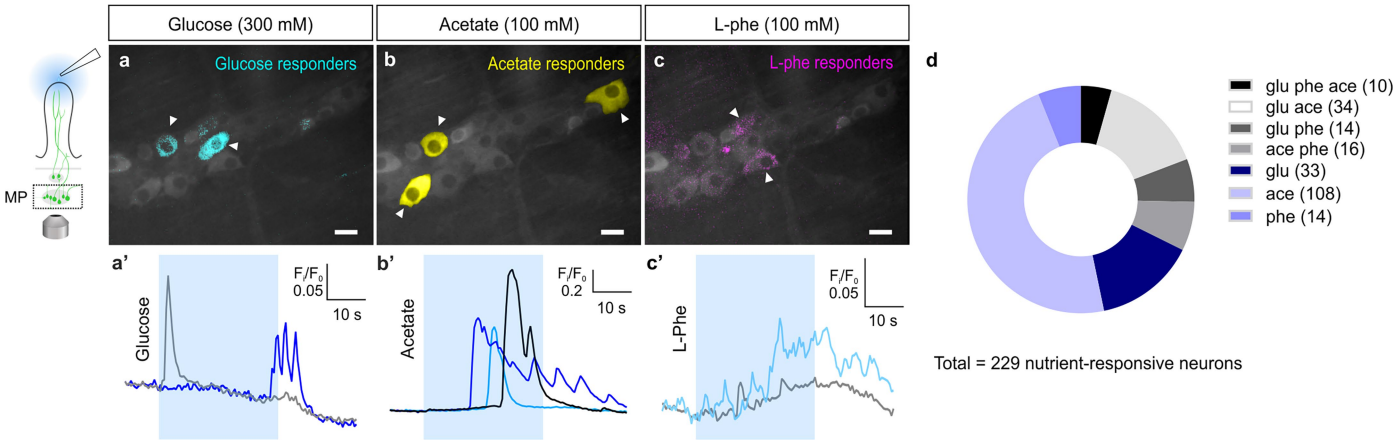

Extended Data Fig. 2 | Myenteric responses to sequentially applied nutrients. **a**–**d**, Sequential application of glucose (300 mM) (**a**,**a'**), acetate (100 mM) (**b**,**b'**) and L-Phe (100 mM) (**c**,**c'**) by mucosal perfusion activates common myenteric neurons as well as neurons that respond uniquely to one nutrient—many neurons responded only to acetate (**d**). *n* = 706 neurons, *N* = 24 preparations examined (13 mice). The specific sequence of nutrient application was alternated between experiments. Each nutrient application was separated by 10 min of Krebs perfusion. Nutrient-responsive neurons are marked by arrowheads. Corresponding Ca^{2+} transients in responding neurons are shown in **a'**–**c'**, Scale bars, 20 µm. Drawing in **a** is adapted from ref. 30 (Wiley).

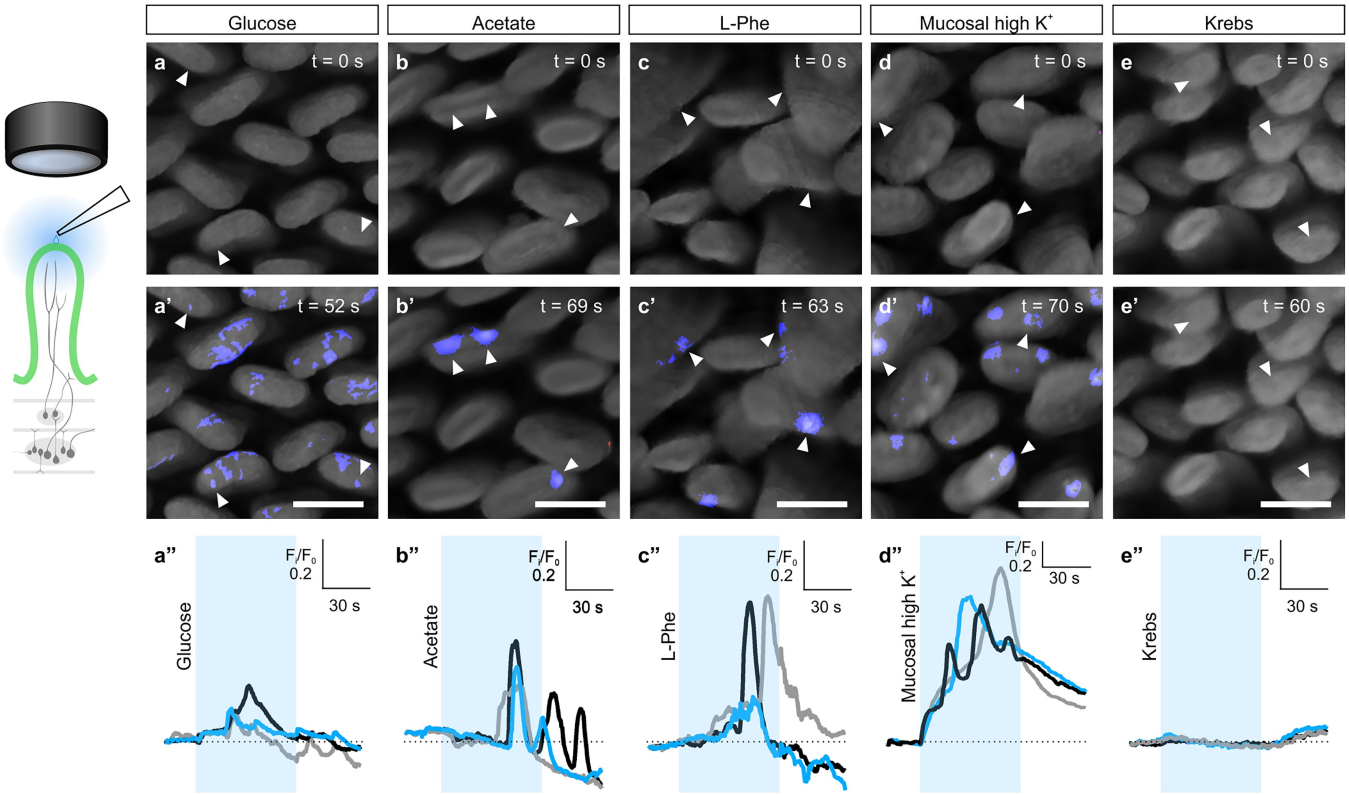

Extended Data Fig. 3 | Nutrients elicit defined epithelial Ca^{2+} responses. **a**–**e'**, Representative wide-field images of the mucosal surface of Villin|GCaMP3 mouse jejunum at baseline ($t = 0$ s) (**a**–**e**) and during the application of **a'**, glucose (300 mM) ($n = 3$ preparations), **b'**, acetate (100 mM) ($n = 3$), **c'**, L-Phe (100 mM) ($n = 3$), **d'**, high K^+ (75 mM) Krebs ($n = 5$) to depolarize the mucosa or **e'**, control Krebs buffer ($n = 3$). Regions of villi that showed an increase in fluorescence intensity in response to each stimulus are highlighted in blue. For each stimulus, examples of Ca^{2+} transients in selected regions of epithelium (arrowheads) are shown at the bottom (**a''**–**e''**). Stimuli were applied from $t = 20$ s to $t = 80$ s. The timing and duration of stimulus application are indicated by the blue boxes. Scale bars, 200 µm. Drawing in **a** is adapted from ref. 30 (Wiley).

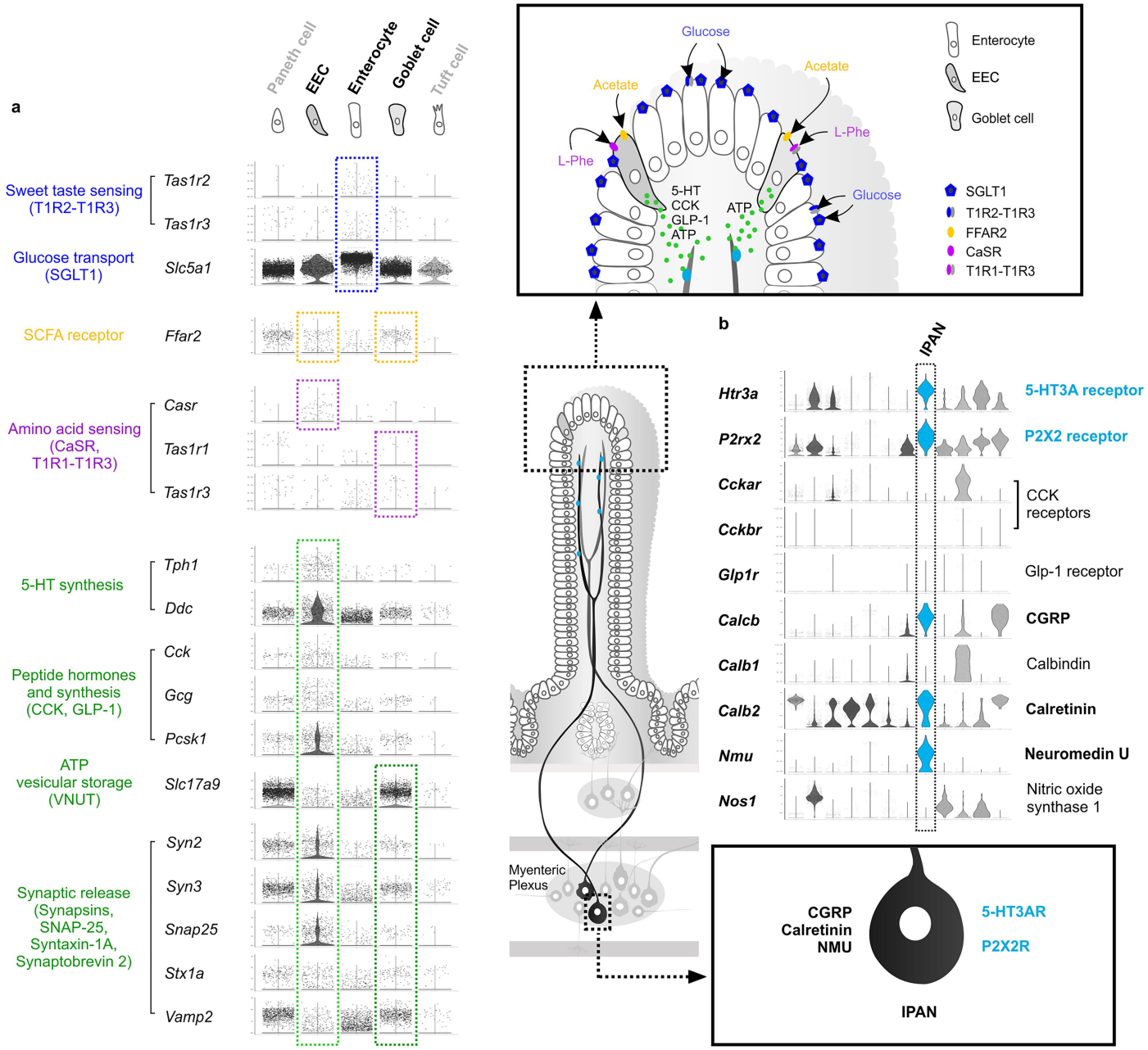

Extended Data Fig. 4 | Expression of genes involved in luminal nutrient signalling in epithelial cells and enteric neurons of the mouse small intestine. a,**b**, Summary of findings extrapolated from single-cell RNA-seq data on small-intestinal epithelium and myenteric neurons sourced from Haber et al.[31] (**a**) and Morarach et al.[27] (**b**), respectively. **a**, Violin plots depicting the differential expression of key genes involved in nutrient signalling across defined epithelial cell types. Genes encoding the sweet taste receptor (T1R2–T1R3) and sodium–glucose co-transporter 1 (SGLT1) (highlighted in blue) are most highly expressed in enterocytes. The free fatty acid receptor 2 (FFAR2; involved in sensing SCFAs e.g. acetate; yellow) is expressed in EECs and goblet cells. Genes encoding the calcium-sensing receptor (CaSR) and T1R1–T1R3, both associated with detecting L-amino acids (e.g. L-Phe; magenta), are expressed in EECs and goblet cells, respectively. EECs also express genes related to synthesis and storage of neuroactive molecules (5-HT, ATP) and peptide hormones (CCK, GLP-1), as well as synaptic release (green). Goblet cells highly express the gene encoding vesicular nucleotide transporter (VNUT; involved in vesicular storage of ATP), along with synaptic protein genes (green). **b**, Violin plots showing enteric neuronal gene expression of receptors corresponding to key signalling mediators expressed by EECs i.e. 5-HT3 receptors, purinergic P2X2 receptors, CCK receptors (CCKAR and CCKBR) and GLP-1 receptors. *5Ht3a* and *P2rx2* were most highly expressed in neurons that express the IPAN markers *Nmu*, *Calcb* and *Calb2* and low levels of *Cckar*, *Cckbr*, *Glp1r*, *Calb1* and *Nos1* expression. Abbreviations: cholecystokinin, CCK; calcitonin gene-related peptide, CGRP; glucagon-like peptide-1, GLP-1. Drawings are adapted from ref. 3 under a Creative Commons licence CC BY 4.0.

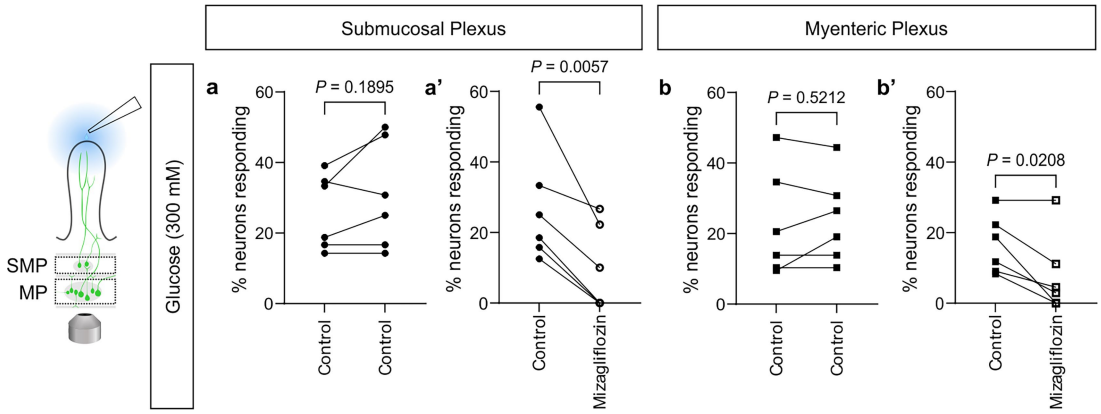

Extended Data Fig. 5 | Submucosal and myenteric responses to luminal glucose are partly mediated by SGLT1. a,**b**, Repeated mucosal glucose (300 mM) application, separated by 10 min Krebs perfusion, evoked reproducible responses in the (**a**) SMP ($n = 6$ FOVs imaged) and (**b**) MP ($n = 6$ FOVs imaged) under control conditions. **a'**, Submucosal ($n = 6$ preparations) and **b'**, myenteric ($n = 6$ preparations) responses to mucosal glucose perfusion were significantly inhibited by mizagliflozin (selective SGLT1 inhibitor, 1 µM; two-sided paired t-test). Drawing in **a** is adapted from ref. 30 (Wiley).

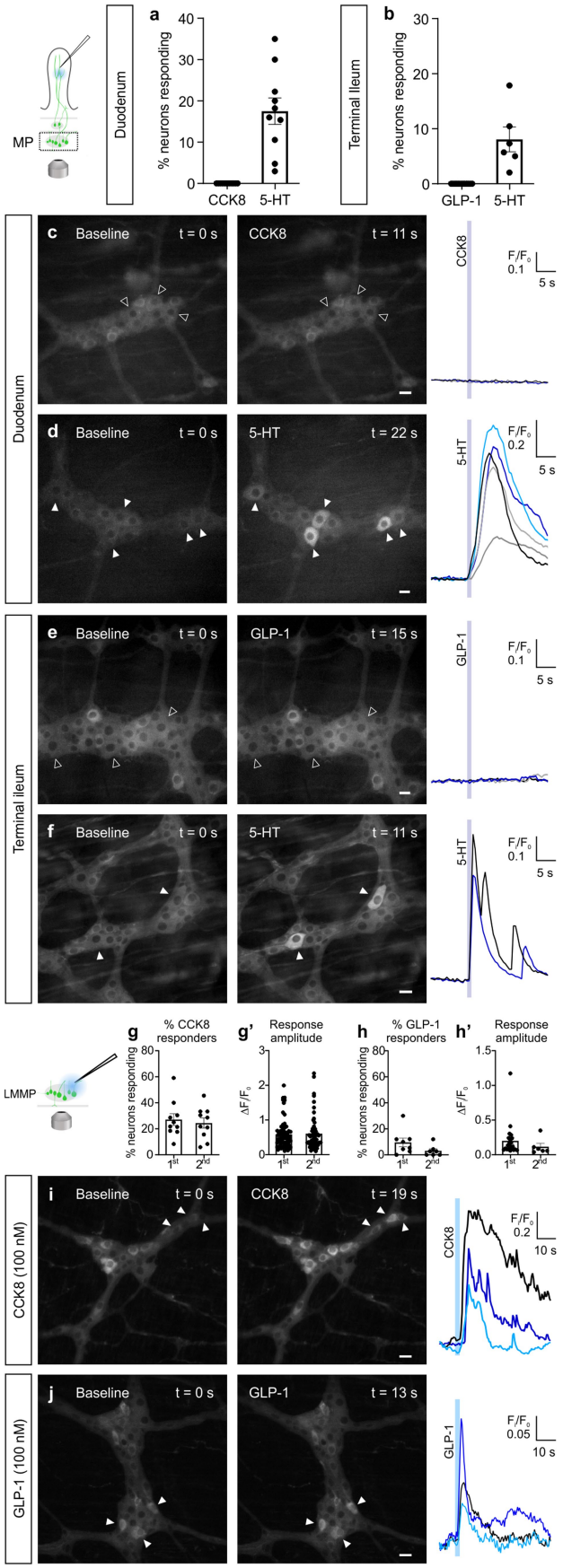

Extended Data Fig. 6 | Myenteric responses to CCK8, GLP-1 and 5-HT in the small intestine. a–**f**, Myenteric responses to intravillus injection of agonists in duodenum (**a**,**c**,**d**) and terminal ileum (**b**,**e**,**f**) full-thickness preparations. While 5-HT (10 µM) evoked neuronal responses in myenteric neurons of both gut regions (**d**, $n = 10$ villi examined; **f**, $n = 6$ villi; responders indicated by arrowheads), no responses were observed to (**c**) CCK8 applied into villi of the duodenum ($n = 12$ villi) or to (**e**) GLP-1 in the villi of terminal ileum ($n = 12$ villi). The traces in the panels on the right show changes in fluorescence intensity over time for neurons indicated by filled arrowheads (responders) or empty arrowheads (non-responders). **g**–**j**, CCK8 (100 nM) or GLP-1 (100 nM) were also applied directly onto myenteric ganglia in peeled jejunum LMMP preparations by pressure ejection from a micropipette at t = 10 s. **g**,**g'**, Two CCK8 applications (separated by a 5 min Krebs washout) evoked reproducible responses in a subset of myenteric neurons ($n = 10$ FOVs examined). **h**,**h'**, Responses to GLP-1 (two applications separated by a 5 min Krebs washout) were less reproducible with only a small percentage of total neurons responding to both applications ($n = 8$ FOVs examined). **i**, Some CCK8-responsive neurons as indicated by arrowheads (left, middle) and corresponding Ca^{2+} transients (right). **j**, Some GLP-1-responsive myenteric neurons as indicated by arrowheads (left, middle) and corresponding Ca^{2+} transients (right). Scale bars, 20 µm. Data are mean ± s.e.m. Drawings in **a** and **g** are adapted from ref. 30 (Wiley).

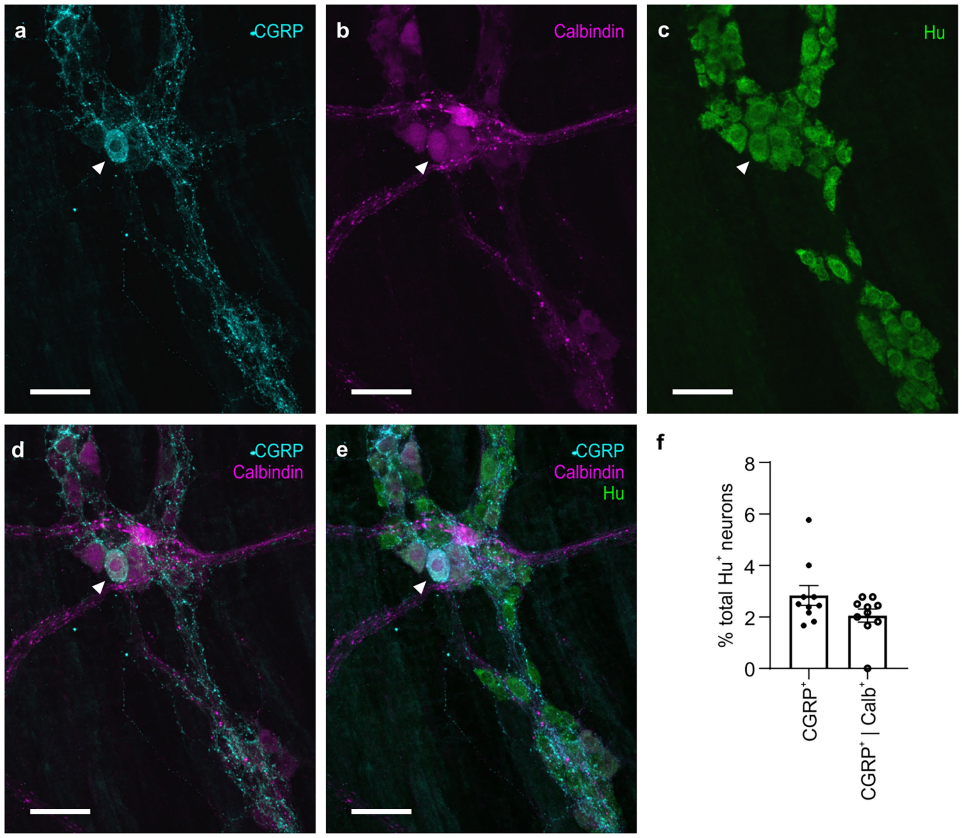

Extended Data Fig. 7 | Myenteric CGRP$^+$ neurons in colchicine-treated tissues show calbindin immunoreactivity. a–**c**, Confocal images of a colchicine-treated LMMP preparation immunolabelled for **a**, calcitonin gene-related peptide (CGRP) (cyan), **b**, calbindin (magenta), and **c**, Hu (pan-neuronal marker; green). **d**,**e**, Merged images illustrating the overlap between CGRP-, calbindin- and/or Hu-immunoreactivity. Scale bars, 50 µm. **f**, Graph showing the percentage of total Hu$^+$ myenteric neurons that are CGRP$^+$ and the percentage of total Hu$^+$ myenteric neurons that are both CGRP$^+$ and calbindin$^+$ (n = 10 FOVs assessed; n = 458 Hu$^+$ neurons, N = 2 mice). Most CGRP-immunoreactive neuronal cell bodies also show calbindin-immunoreactivity. Data are mean ± s.e.m.

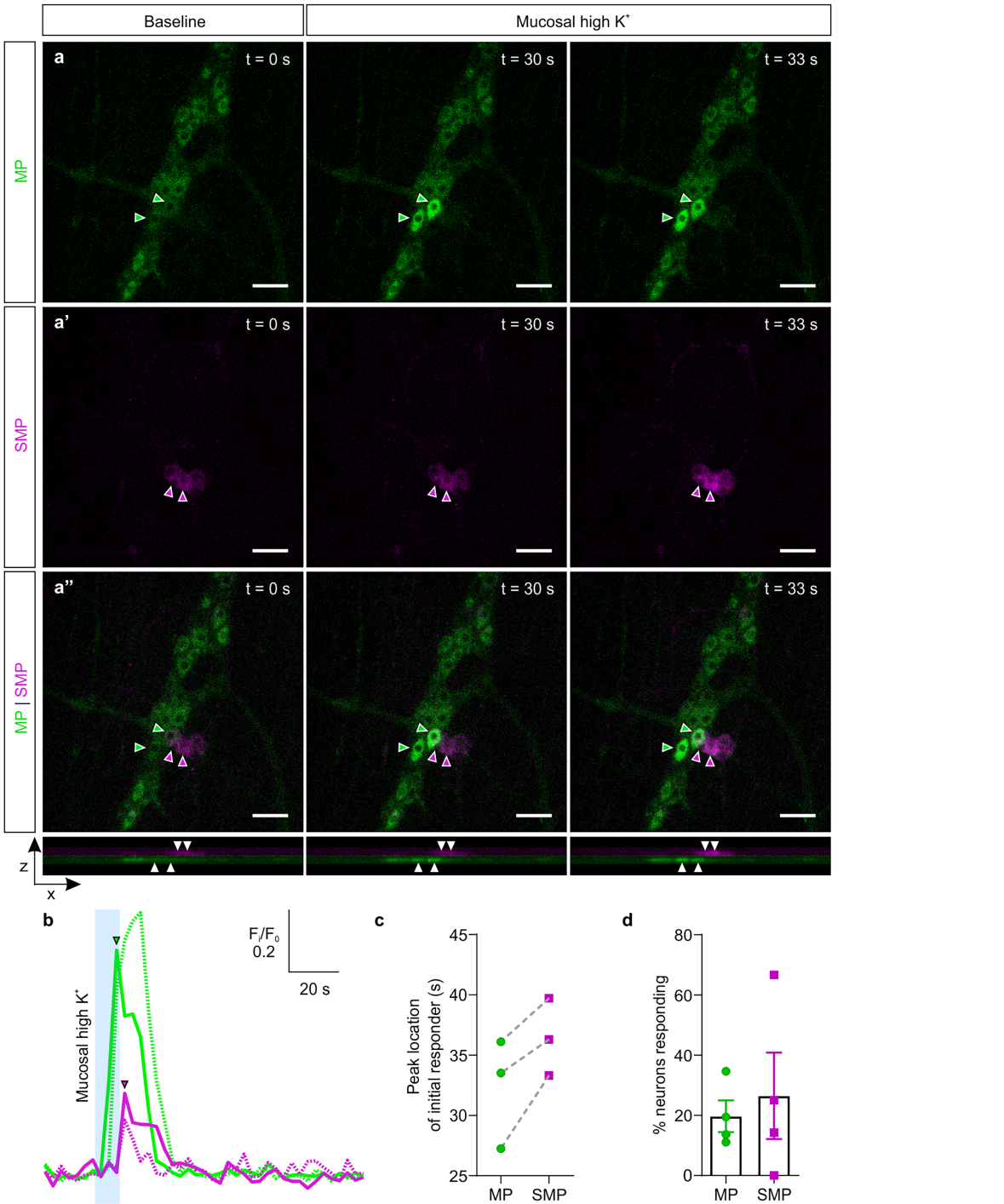

Extended Data Fig. 8 | Timing of myenteric and submucosal responses to mucosal high K$^+$. a–a″, Representative spinning disk confocal microscope recording of Ca^{2+} activity in the MP and SMP in response to mucosal high K^+ application (from t = 20 s to t = 30 s). Maximum XY projections of the Z stack (25 µm) divided into the (**a**) MP and (**a′**) SMP. **a″**, Maximum XY and XZ projections of the full stack with the MP and SMP depth colour-coded in green and magenta, respectively. Scale bars, 50 µm. Responding neurons are indicated by colour-coded arrowheads. **b**, Corresponding traces of Ca^{2+} responses in the myenteric (green) and submucosal neurons (magenta) indicated in **a–a″**, depicted as a change in fluorescence over time. Arrowheads mark the Ca^{2+} peak of the initial responders. **c**, The Ca^{2+} peak of the first myenteric neuron that responded consistently preceded that of the first submucosal neuron that responded in corresponding preparations ($n = 3$). **d**, The percentage of myenteric and submucosal neurons that responded to mucosal high K^+ ($n = 3$ preparations). Data are mean ± s.e.m.

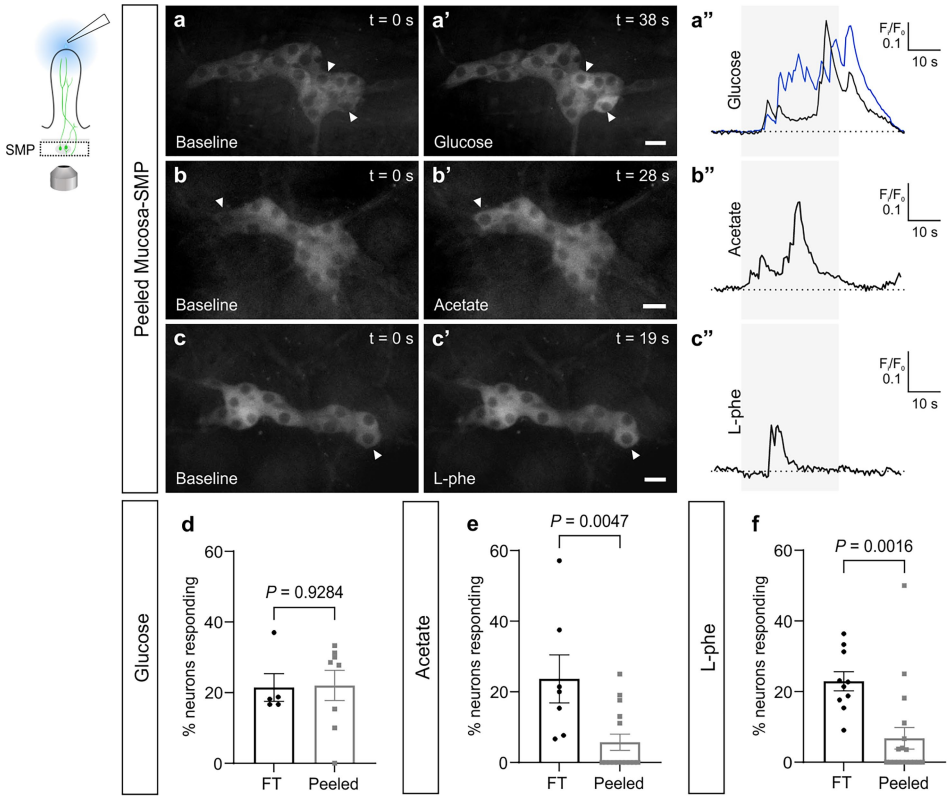

Extended Data Fig. 9 | Submucosal responses to nutrients perfused onto the mucosa in peeled preparations. a–c'', Nutrient responses in peeled mucosa–SMP preparations. a,a', Mucosal perfusion of glucose (300 mM) activates a subset of submucosal neurons as marked by white arrowheads. Glucose was applied from $t = 10$ s to $t = 40$ s. a'', Corresponding Ca^{2+} transients in the responding neurons indicated in the previous panels. b–b'', Mucosal perfusion of acetate (100 mM) activates a subset of submucosal neurons as marked by white arrowheads. Acetate was applied from $t = 10$ s to $t = 40$ s. c–c'', Mucosal perfusion of L-Phe (100 mM) activates a subset of submucosal neurons as marked by white arrowheads. Acetate was applied from $t = 10$ s to $t = 40$ s. Scale bars, 20 µm. d–f, Nutrient responders in the SMP of full-thickness (FT) preparations versus peeled preparations with the MP removed. While the percentage of submucosal responders to d, glucose were comparable (peeled: $n = 8$ FOVs examined; FT: $n = 5$ FOVs), fewer responders were observed in response to e, acetate and f, L-Phe in peeled preparations compared to in FT preparations (two-sided unpaired t-test; acetate, peeled: $n = 15$ FOVs, FT: $n = 7$ FOVs; L-Phe, peeled: $n = 18$ FOVs, FT: $n = 10$ FOVs). Data are mean ± s.e.m. Drawing in a is adapted from ref. 30 (Wiley).

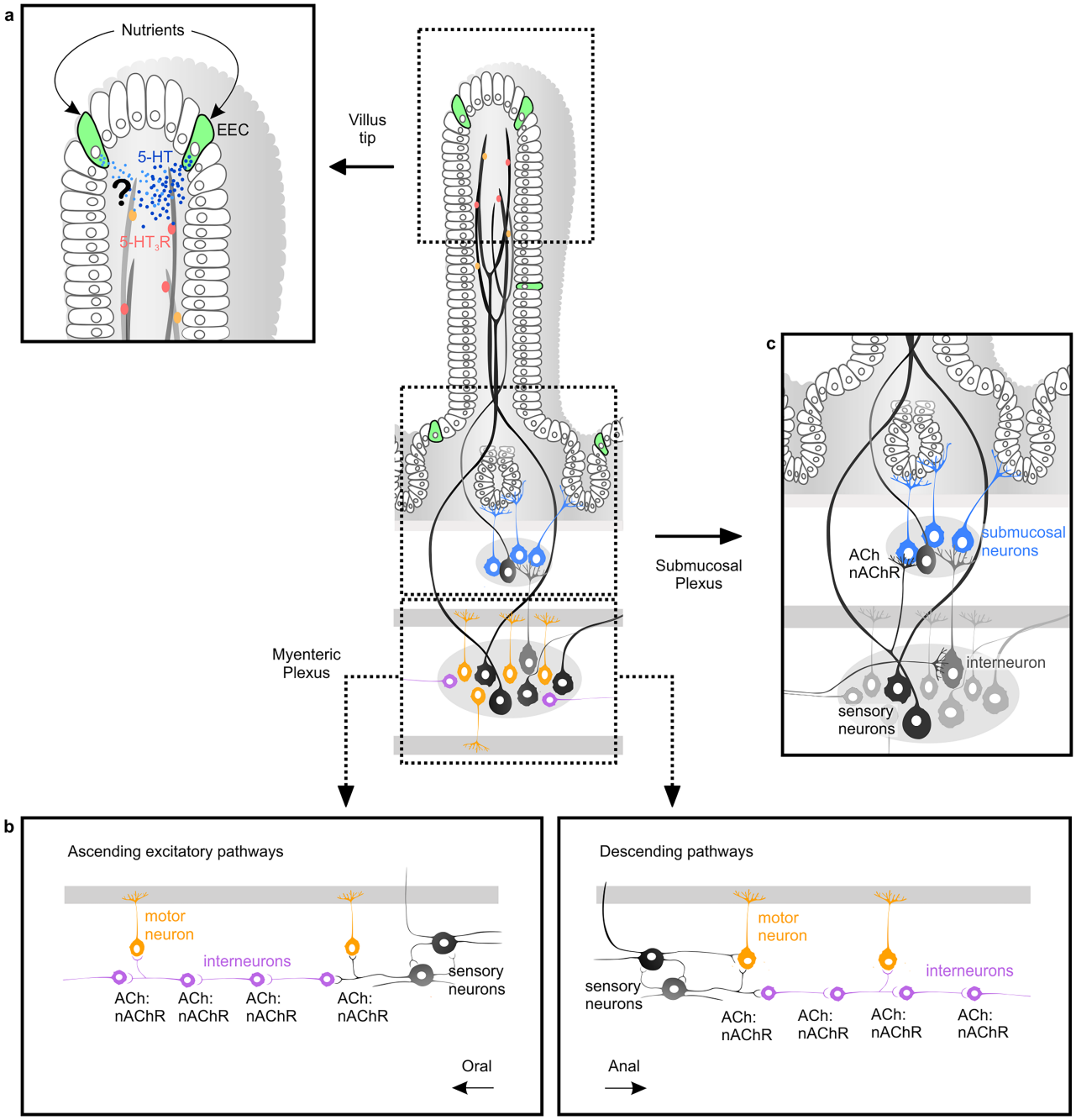

Extended Data Fig. 10 | Simplified schematic of proposed model for the detection of luminal nutrient information by the ENS of the mouse small intestine. a, Luminal nutrients are first detected at the mucosal surface by enteroendocrine (EEC) cells, which include EC cells, as well as other epithelial cells such as enterocytes. The basolateral release of 5-HT from EC cells after nutrient activation then stimulates 5-HT_3 receptor (5-HT_3R)-expressing intrinsic sensory nerve endings that supply the villi. Other mucosal mediators that activate intrinsic nerve endings and their corresponding neuronal receptors have yet to be established. Schematic adapted from ref. 3 under a Creative Commons licence CC BY 4.0. **b**, Intrinsic sensory neurons (IPANs) that project to the mucosa reside in the MP and respond mainly to the luminal stimulus. Interneurons and motor neurons of ascending excitatory and/or inhibitory descending pathways may be activated secondarily through nicotinic transmission. **c**, IPANs are also found in the SMP and respond directly to luminal stimuli. Other submucosal (secretomotor) neurons respond secondarily through interneurons and/or myenteric sensory neurons, and their responses are mediated by nicotinic transmission.

nature portfolio

Corresponding author(s): Pieter Vanden Berghe

Last updated by author(s): Apr 25, 2025

Reporting Summary

Nature Portfolio wishes to improve the reproducibility of the work that we publish. This form provides structure for consistency and transparency in reporting. For further information on Nature Portfolio policies, see our Editorial Policies and the Editorial Policy Checklist.

Statistics

For all statistical analyses, confirm that the following items are present in the figure legend, table legend, main text, or Methods section.

n/a	Confirmed
☐	☒ The exact sample size (*n*) for each experimental group/condition, given as a discrete number and unit of measurement
☐	☒ A statement on whether measurements were taken from distinct samples or whether the same sample was measured repeatedly
☐	☒ The statistical test(s) used AND whether they are one- or two-sided *Only common tests should be described solely by name; describe more complex techniques in the Methods section.*
☐	☒ A description of all covariates tested
☐	☒ A description of any assumptions or corrections, such as tests of normality and adjustment for multiple comparisons
☐	☒ A full description of the statistical parameters including central tendency (e.g. means) or other basic estimates (e.g. regression coefficient) AND variation (e.g. standard deviation) or associated estimates of uncertainty (e.g. confidence intervals)
☐	☒ For null hypothesis testing, the test statistic (e.g. *F*, *t*, *r*) with confidence intervals, effect sizes, degrees of freedom and *P* value noted *Give P values as exact values whenever suitable.*
☒	☐ For Bayesian analysis, information on the choice of priors and Markov chain Monte Carlo settings
☒	☐ For hierarchical and complex designs, identification of the appropriate level for tests and full reporting of outcomes
☒	☐ Estimates of effect sizes (e.g. Cohen's *d*, Pearson's *r*), indicating how they were calculated

Our web collection on statistics for biologists contains articles on many of the points above.

Software and code

Policy information about availability of computer code

Data collection	Widefield Ca2+ imaging recordings of ENS were acquired using TILLVISION software (TILL Photonics; v4.01) and epithelium recordings were acquired using HC ImageLive software (Hamamatsu; v4.4.2.7), fluorescence images of post-hoc immunostainings and RNAscope labelled preparations were acquired using Olympus DP2-TWAIN software (v8.2) or ZEN blue (v3.7.97.05000), spinning disk confocal images were acquired using Andor iQ software (v2.9.1), confocal images were taken using Zeiss ZEN 2012 SP5 FP3 (black edition; v14.0.27.201) and ZEN 2.3 SP1 FP3 (black edition; v14.0.29.201).
Data analysis	Analysis of Ca2+ imaging recordings were performed using Igor Pro (Wavemetrics) with custom-written routines (already published via Li et al. 2019 Elife. DOI:https://doi.org/10.7554/eLife.26850) , and in Fiji (Image J version 2.1.0/1.53t). Published scRNAseq datasets were analysed in R (v.4.1.2) using the Seurat (v4.1.0) package. Statistical analyses were performed using GraphPad Prism.

For manuscripts utilizing custom algorithms or software that are central to the research but not yet described in published literature, software must be made available to editors and reviewers. We strongly encourage code deposition in a community repository (e.g. GitHub). See the Nature Portfolio guidelines for submitting code & software for further information.

Data

Policy information about availability of data

All manuscripts must include a data availability statement. This statement should provide the following information, where applicable:

- Accession codes, unique identifiers, or web links for publicly available datasets
- A description of any restrictions on data availability
- For clinical datasets or third party data, please ensure that the statement adheres to our policy

All data are available in the main text or the supplementary materials.

Human research participants

Policy information about studies involving human research participants and Sex and Gender in Research.

Reporting on sex and gender	*Use the terms sex (biological attribute) and gender (shaped by social and cultural circumstances) carefully in order to avoid confusing both terms. Indicate if findings apply to only one sex or gender; describe whether sex and gender were considered in study design whether sex and/or gender was determined based on self-reporting or assigned and methods used. Provide in the source data disaggregated sex and gender data where this information has been collected, and consent has been obtained for sharing of individual-level data; provide overall numbers in this Reporting Summary. Please state if this information has not been collected. Report sex- and gender-based analyses where performed, justify reasons for lack of sex- and gender-based analysis.*
Population characteristics	*Describe the covariate-relevant population characteristics of the human research participants (e.g. age, genotypic information, past and current diagnosis and treatment categories). If you filled out the behavioural & social sciences study design questions and have nothing to add here, write "See above."*
Recruitment	*Describe how participants were recruited. Outline any potential self-selection bias or other biases that may be present and how these are likely to impact results.*
Ethics oversight	*Identify the organization(s) that approved the study protocol.*

Note that full information on the approval of the study protocol must also be provided in the manuscript.

Field-specific reporting

Please select the one below that is the best fit for your research. If you are not sure, read the appropriate sections before making your selection.

☒ Life sciences ☐ Behavioural & social sciences ☐ Ecological, evolutionary & environmental sciences

For a reference copy of the document with all sections, see nature.com/documents/nr-reporting-summary-flat.pdf

Life sciences study design

All studies must disclose on these points even when the disclosure is negative.

Sample size	Literature in the field and experience were used to determine the approximate number of neurons, preparations, and animals needed for experiments. No formal sample size calculation was performed, as this is the first study to investigate the effect of nutrient activation of enteric neurons in intact tissues. At least three animals were used per experiment. Depending on the specifics of certain experiments, where more or less biological variability was expected, the number of animals was increased to achieve the same power. All experiments included animals of the same genetic background to reduce variation. The exact number of biological or technical replicates (animals, tissue preparations, neurons, and/or fields of view imaged, where appropriate) is reported in the manuscript text.
Data exclusions	Samples with poor immunohistochemical staining quality were excluded from further analysis. Unhealthy enteric neurons/ganglia (nuclear GCaMP fluorescence) or instances where recordings in which image registration fails to correct for tissue contraction were excluded from Ca2+ imaging analyses.
Replication	All the measurements that didn't require statistical testing were taken from at least 2 animals in independent experiments (otherwise at least 3). All replication attempts were successful (except cases listed as reason for exclusion).
Randomization	Animals from different litters were randomly assigned and used across different experiments.
Blinding	No biological groups of animals, or pathological or treatment conditions were compared in these experiments and therefore did not require blinding.

Reporting for specific materials, systems and methods

We require information from authors about some types of materials, experimental systems and methods used in many studies. Here, indicate whether each material, system or method listed is relevant to your study. If you are not sure if a list item applies to your research, read the appropriate section before selecting a response.

Materials & experimental systems

n/a	Involved in the study
☐	☒ Antibodies
☒	☐ Eukaryotic cell lines
☒	☐ Palaeontology and archaeology
☐	☒ Animals and other organisms
☒	☐ Clinical data
☒	☐ Dual use research of concern

Methods

n/a	Involved in the study
☒	☐ ChIP-seq
☒	☐ Flow cytometry
☒	☐ MRI-based neuroimaging

Antibodies

Antibodies used

VIP Rabbit 1:1000 Millipore (AB982)
ChAT Goat 1:500 Chemicon (AB144P)
nNOS Sheep 1:1000 Gift from Dr. P. Emson
Calbindin D-28k Rabbit 1:1600 Swant (cb-38a)
CGRP Goat 1:1000 BioRad (1720-9007)
HuCD Mouse 1:500 Molecular Probes (A21271)
HuCD Human 1:5000 Gift from Thomas J Kryzer
GFP Rat 1:400 Nacalai Tesque (04404-84)

Anti-goat AF594 Donkey 1:1000 Invitrogen (A11058)
Anti-goat Cy3 1:500 Jackson Immuno Labs (705-165-147)
Anti-sheep AF647 Donkey 1:500 Molecular Probes (A21448)
Anti-rabbit AF594 Donkey 1:500 Molecular Probes (A21207)
Anti-rabbit AF674 Donkey 1:500 Jackson Immuno Labs (711-605-152)
Anti-mouse AMCA Donkey 1:250 Jackson Immuno Labs (715-155-151)
Anti-human AF488 Donkey 1:1000 Jackson Immuno Labs (709-545-149)
Anti-rat AF488 Donkey 1:500 Invitrogen (A21208)

Validation

VIP Millipore (AB982) was validated by the manufacturer for immunohistochemistry application and reactivity against mouse; reactivity against mouse tissue was observed in this manuscript
ChAT Chemicon (AB144P) was validated by the manufacturer for immunohistochemistry application and reactivity against mouse; reactivity against mouse tissue was observed in this manuscript
nNOS (Gift from Dr. P.C. Emson - The Babraham Institute, Cambridge, UK) has been widely used in other published studies (Parathan et al., 2020 Developmental Biology; Spencer et al., 2018 J Neurosci; Sander et al., 2003 J Histochem Cytochem); reactivity against mouse tissue was observed in this manuscript
Calbindin D-28k Swant (cb-38a) was validated by the manufacturer for immunohistochemistry application and reacts with mouse. This antibody has been reported to cross-react with CALR based on cross-validation with different antibodies, literature and scRNAseq data (Morarach et al. Nature Neuroscience 2021)
CGRP BioRad (1720-9007) was validated by the manufacturer for immunohistochemistry application and reactivity against mouse; reactivity against mouse tissue was observed in this manuscript
HuCD Molecular Probes (A-21271) was validated by the manufacturer for immunohistochemistry application and reacts against mouse; reactivity against mouse tissue was observed in this manuscript
HuCD (Dr. Vanda Lennon, Mayo clinic) has been widely used in other published studies (Hao et al., 2013 J Comp Neurol; Rao et al., 2017 Gastroenterology; Cheng et al., 2017 J Surg Res.); reactivity against mouse tissue was observed in this manuscript
GFP Rat 1:400 Nacalai Tesque (04404-84) was validated by the manufacturer for immunohistochemistry application and reacts against mouse; reactivity against mouse tissue was observed in this manuscript and has been reported in published studies (Boesmans et al., 2019 Glia; Laddach et al., 2023 Nature Communications)

Anti-goat AF594 Donkey 1:1000 Invitrogen (A-11058) was validated by the manufacturer for immunohistochemistry application
Anti-goat Cy3 1:500 Jackson Immuno Labs (705-165-147) was validated by the manufacturer for immunohistochemistry application
Anti-sheep AF647 Donkey 1:500 Molecular Probes (A-21448) was validated by the manufacturer for immunohistochemistry application
Anti-rabbit AF594 Donkey 1:500 Molecular Probes (A-21207) was validated by the manufacturer for immunohistochemistry application
Anti-rabbit AF674 Donkey 1:500 Jackson Immuno Labs (711-605-152) was validated by the manufacturer for immunohistochemistry application
Anti-mouse AMCA Donkey 1:250 Jackson Immuno Labs (715-155-151) was validated by the manufacturer for immunohistochemistry application
Anti-human AF488 Donkey 1:1000 Jackson Immuno Labs (709-545-149) was validated by the manufacturer for

immunohistochemistry application
Anti-rat AF488 Donkey 1:500 Invitrogen (A21208) was validated by the manufacturer for immunohistochemistry application

Animals and other research organisms

Policy information about studies involving animals; ARRIVE guidelines recommended for reporting animal research, and Sex and Gender in Research

Laboratory animals	Adult mice (at least 6 weeks of age) were used in this study. Wnt1-Cre;R26R-LsL-GCaMP3 and Villin-cre;R26R-LsL-GCaMP3 mice were used for calcium imaging experiments. Wnt1-Cre;R26R-LsL-GCaMP3 mice were used for DiI labelling experiments. C57BL/6 mice were used for CGRP-immunolabelling experiments involving colchicine-treatment.
Wild animals	N/A
Reporting on sex	Both male and female mice were used in this study and were randomly assigned across different experiments. Thus, findings apply to to both sexes. Examining potential sex-specific differences was beyond the scope of this study, thus data were not disaggregated for sex.
Field-collected samples	N/A
Ethics oversight	All animal procedures are approved by the Animal Ethics Committee of the University of Leuven (Belgium).

Note that full information on the approval of the study protocol must also be provided in the manuscript.